Theses and Dissertations   Graduate School

2006

A Model for Studying Vasogenic Brain Edema

Anshu Shukla
Virginia Commonwealth University

A MODEL FOR STUDYING VASOGENIC BRAIN EDEMA

A thesis submitted in partial fulfillment of the requirements for the degree of Master of Science at Virginia Commonwealth University.

by

ANSHU SHUKLA

B.S. Biomedical Engineering, Electrical Engineering, Economics, Duke University, 2002
Certificate Anatomy and Neurobiology, Virginia Commonwealth University, 2005

Director: William C. Broaddus
Hord Associate Professor
Departments of Neurosurgery, Department of Anatomy & Neurobiology

Virginia Commonwealth University
Richmond, Virginia
August 2006

Acknowledgements

Table of Contents

List of Figures

Abstract

A MODEL FOR STUDYING VASOGENIC BRAIN EDEMA

By Anshu Shukla, B.S.E.

A thesis submitted in partial fulfillment of the requirements for the degree of Master of Science at Virginia Commonwealth University.

Virginia Commonwealth University, 2006

Major Director: William C. Broaddus, M.D., Ph.D., Hord Associate Professor
Department of Neurosurgery, Department of Anatomy & Neurobiology

Convection-enhanced delivery (CED) is a proven method for targeted drug delivery to the brain that circumvents the blood-brain barrier (BBB). Little study has been conducted in understanding CED in pathological brain states. This is of importance when dealing with chemotherapeutic agent delivery to brain tumors, where vasogenic edema (VE) exists. The current study aims to characterize a model of VE suitable for studying CED.

VE was produced in the right hemisphere of the rat brain using multiple infusions of hyperosmotic mannitol (0.25mL/kg/s over 30 seconds) delivered through the right

internal carotid artery. Magnetic resonance imaging (MRI) revealed consistent edema formation and high water levels in the ipsilateral gray and white matter within an hour of the first infusion. Evan's Blue (EB) staining verified that VE has formed. However, apparent diffusion coefficient (ADC) and histological examination revealed also that some possible cytotoxic edema formed.

This model provides a reproducible technique for generating a large area of edema for CED study. Further studies with lower doses of mannitol, while titrating to changes in ADC and values for fractional water content, may modify this model with a greater component of VE and less cerebral toxicity.

CHAPTER 1

PATHOLOGICAL BRAIN STATES AND CONVECTION-ENHANCED

DELIVERY

For a variety of pathological brain states, such as traumatic brain injury (TBI),

ischemic stroke and tumors, systemic delivery of therapeutic agents to the brain is a

problem due to the blood-brain barrier (BBB).[1] Techniques such as convection-enhanced

delivery (CED) can by-pass the BBB; however the above conditions involve a significant

element of edema formation[2] that can affect accurate dosing via CED.[3]

TBI, stroke and tumors generally have two types of edema associated with them:

cytotoxic edema (CE) and vasogenic edema (VE).[4-8] CE develops when cells of the brain

lack an energy supply and suffer from a breakdown of ion-transport. The increased levels

of intracellular sodium lead to increased water content and subsequent cellular swelling.[9;10]

The intracellular swelling causes the extracellular space (ECS) to contract when compared

to normal brain. VE develops as a result of BBB breakdown and a build-up of water in the

ECS,[2] and can be characterized by ECS expansion. Diagrams outlining the ECS changes

in both VE and CE are shown in **Figure 1-1**.

Figure 1-1. Diagram illustrating extracellular space morphology under conditions of vasogenic and cytotoxic edema. **A:** Normal brain tissue. **B:** Vasogenic edema exhibits extracellular space expansion. **C:** Cytotoxic edema is characterized by shrinkage of the extracellular space. The intracellular spaces are shaded for clarity. (Diagrams courtesy of P. Haar[3])
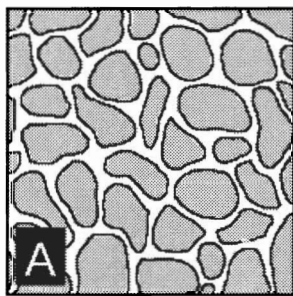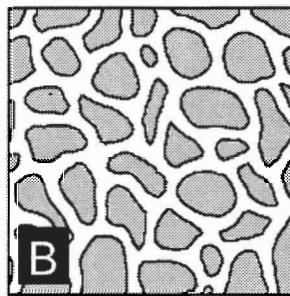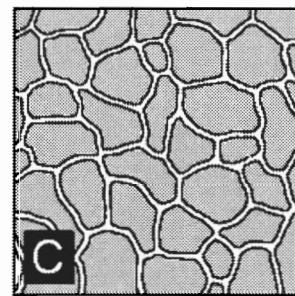
Normal   Vasogenic Edema   Cytotoxic Edema

Studies have found that TBI has an acute VE development, with the BBB opening and closing within 30 minutes of injury.[11] Increased apparent diffusion coefficient (ADC) values obtained from magnetic resonance imaging (MRI) are sensitive to water protons in the ECS. Elevated ADC values, consistent with VE, were found up to a period of 45 minutes post-injury in rats, however these values fell to below normal values and remained low for weeks afterward, consistent with predominantly CE in this phase after injury.[4;5] Therefore, the edema seen in TBI is mostly CE in nature. In ischemic brain injury, there is acute CE development from cellular damage followed by some mixture of VE development several hours post-injury.[6;12] Tumors generally exhibit a high degree of VE in the peritumoral tissue.[8] Some CE may be present due to ischemic anoxia in rapidly growing tumors where vasculature does not keep up with the cells.[13;14] Specific mechanisms behind VE formation will be discussed in the next chapter.

A common and devastating form of brain tumor is glioblastoma multiforme (GBM), which accounts for 50% of adult gliomas.[15] GBM is classified by the World Health Organization (WHO) as a grade IV astrocytoma,[16] and is seen in 9,000 U.S. cases annually with an incidence of 3 per 100,000 per year.[15] The highest incidence of GBM occurs in the elderly and white males.[17] Even with the combination of surgery, chemotherapy, and radiation, the average survival time for patients is less than 2 years.[18]

GBM is seen in two forms: (1) a primary form which develops directly from glial cells, and (2) a secondary form which is thought to develop form from low-grade astrocytomas that are already present in tissue.[17] The primary form is more aggressive and invasive and is seen in an older population of individuals (median age = 62.2 years), while

the secondary form tends to arise in relatively younger patients (median age = 44.9 years).[16;19] Regardless of pathway, the clinical signs of GBM remain the same: rapid proliferation, diffuse invasion, angiogenesis, and tissue necrosis.[16] Surrounding the tissue is a region of peritumoral edema (PTE) which is VE in nature due to disruption of the BBB in surrounding vasculature, and results in widening of the ECS, [14;20] the mechanism of which is discussed in a later chapter. GBM cannot be cured by surgery but surgical removal is the primary goal with such a high grade tumor, which is then followed by a combination of radiotherapy and chemotherapy.[15]

Chemotherapeutic treatment of brain tumors is challenging via normal vascular drug delivery due to the BBB.[21] The normal BBB functions by preventing passage of water soluble drugs that have a molecular weight greater than 180, whereas most chemotherapeutic agents that are currently being used have a molecular weight between 200 and 1200.[21] Lipid solubility, charge, and molecular mass are the most important factors that determine if a drug can cross the BBB.[21] By circumventing the BBB, CED is an effective approach to targeted delivery of chemotherapeutic agents.[1;22;23] CED involves a catheter being placed directly into parenchymal tissue and the desired therapeutic agent is slowly infused into the region via a pump mechanism (**Figure 1-2 A**). CED of toxins has been used to treat gliomas.[15;24] In addition, CED of chemotherapeutics such as Taxol[25] and liposomes[1] has been used.

CED should not be confused with direct stereotactic inoculation. The latter technique creates a limited volume of distribution in the brain tissue (V_t) and therefore reduces the agent's therapeutic utility.[21] The V_t of the drug can be increased via fluid

convection under a constant pressure gradient.[21;26] Thus, the drug distribution relies on

the bulk flow of the fluid within the ECS of the brain. Bobo *et al.* found that by using a

bulk-flow technique, they could infuse [^{14}C] sucrose (M_r, 359) and ^{111}In-labeled transferrin

(M_r, 80,000) into the internal capsule of cats under low but constant pressure.[27] They

demonstrated a linear increase in V_t that correlated with volume of infusion. CED is

promising for clinical use, and can help circumvent the problem of poor drug delivery

when studying other chemotherapeutic agents derived from growth factors, genetic vectors,

enzymes, neurotrophic factors, and antibodies.[27] In addition to agents mentioned above,

CED has been used to deliver antisense oligonucleotides.[28-30] CED is also applicable in

treating Parkinson's disease and other diseases associated with local or regional brain

abnormalities. [1;21;22;31]

Since agents delivered to the brain via CED will distribute through the ECS,

pathological states affecting the ECS will directly affect drug distribution. As mentioned

above, peritumoral tissue exhibits VE and some CE.[14;20] Therefore, understanding CED

distribution under pathological condition of VE is vital for accurate drug dosing and

delivery. The behavior of infusate under conditions of CE has been well characterized in

studies conducted by Haar, however the same studies showed inconclusive results for CED

in a model of VE utilizing prior direct intraparenchymal infusion of albumin.[3]

VE leads to an expansion of ECS and an increase in the volume fraction. As noted

in studies conducted by Haar, this condition would lead to an increase in the amount of

available space for the infused medication to occupy.[3] Therefore, it will be likely that when

equal volumes of infusate are applied to a normal brain and one suffering from VE, the

edematous brain tissue exhibits lower tissue distribution volume and higher tissue

concentration of infusate (**Figure 1-2 B**).[3]

The intracellular swelling seen in CE causes a reduction in ECS and decrease in

volume fraction. Haar expected that the Gd-DTPA infusate would expand to a higher

tissue volume with lower tissue concentration given less ECS to occupy (**Figure 1-2 C**).

This hypothesis was successfully proved correct via experimentation.[3]

To investigate CED in different types of edema, Haar utilized rat brains to model

conditions of VE via direct interparenchymal albumin infusion, and CE via the middle

cerebral artery (MCA) occlusion model.[3] Gadolinium-diethylene-triamine penta-acetic acid

(Gd-DTPA) was used as a model therapeutic agent for CED. Haar found, as expected, CE

led to a significantly higher volume of agent distribution with lower tissue concentrations

of infusate when compared to normal brain tissue (**Figure 1-2C**).[3] However, the volume of

distribution and tissue concentration of Gd-DTPA did not change as expected in the VE

model. In fact, the changes followed a similar pattern as seen in CE, although they were

not significantly different from normal brain tissue and substantial variability in the data

was noted. Haar cited the possibility that the needle used to infuse albumin 24 hours prior

to Gd-DTPA infusion may have promoted "escape" of infusate along this track and might

have acted as a stab wound, which could have led to CE development. [3]

Haar also noted a high degree of variance in the results. These were statistically

different and attributed to either of two observed scenarios: (1) the infusate quickly

diffused to a large tissue volume, or (2) a rapid retrograde flow of infusate. Haar explained

Figure 1-2. Diagram illustrating infusion under conditions of vasogenic and cytotoxic edema. **A:** Diagram of infusion in normal brain. **B:** Diagram of possible infusion in brain tissue with vasogenic edema in which the increased extracellular space creates a smaller volume of infusion, thereby decreasing the tissue infusate concentration. **C:** Diagram illustrating infusion in brain tissue with cytotoxic edema in which the decreased extracellular space creates a larger volume of infusion and effectively decreases tissue infusate concentrations. (Diagrams courtesy of P. Haar[3])

Normal   Vasogenic Edema   Cytotoxic Edema
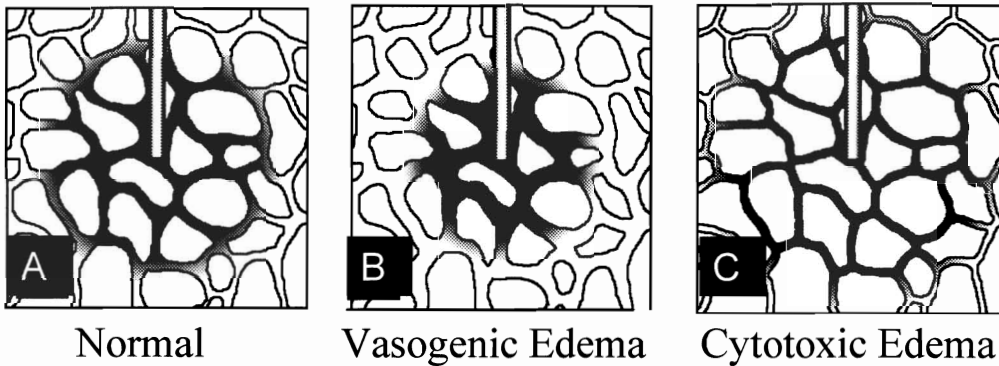
the latter scenario as possibly due to back flow up a fluid channel around the cannula tract so that it collected in the corpus callosum.[3] Haar's results suggest that VE can cause either increased interstitial pressure in the ECS thereby forcing the infusate back up the cannula tract, or existing edematous conditions weakens the seal between the infusion cannula and surrounding tissue to allow backflow.[3]

The VE model utilized in Haar's experiment presented some limitations that may have confounded the inconclusive results. These limitations were stated by the author as the small brain size, crossing of both albumin and Gd-DTPA infusion tracts and proximity of the infusion cannula to white matter.[3] Due to these limitations and the invasive nature of the model, albumin infusion presents itself as an impractical and incompatible model for studying CED in the rat brain. Therefore, a better model of VE is needed in order to study CED in VE. The goal of the present study was to analyze an alternative model of VE in rodent brain that would be less intrusive and provide a consistent region of edema development in order to study its effects on CED.

CHAPTER 2

VASOGENIC EDEMA AND THE BLOOD-BRAIN BARRIER

Pathological brain states such as traumatic brain injury (TBI), stroke, and tumors can produce different types of brain edema.[2] CE results from hypoxic conditions in ischemic areas of the brain. Specifically, a breakdown in ion transport across the cell membranes leads to a build-up of ions within the cells. As water migrates into the intracellular environment, there is a marked degree of astrocytic and neuronal swelling.[32-34] Under conditions of CE, the cells swell as water accumulates inside of them. This expansion of intracellular space can lead to a subsequent 75% contraction of ECS.[35;36] This change in ECS is depicted schematically in **Figure 1-1 C.**

VE is commonly found in patients who suffer from intracranial tumors, severe head injury, cerebral ischemia, hemorrhagic stroke and CNS infections.[2] These conditions can lead to a breakdown in the BBB thereby increasing the permeability of local microvessels. The BBB protects the brain and maintains homeostasis in the brain. Disruption of the BBB results in a leakage of serum components into the parenchyma. This plasma leakage is due to the inherent pressure gradient between the vascular space and ECS.[2] The protein-rich fluid spreads by bulk flow and by accumulating into the extracellular compartment of the brain, can lead to cerebral swelling, compression and displacement of the brain stem,

increased intracranial pressure (ICP), systemic hypertension and cardio respiratory collapse.[2;37;38] The presence of serum water and oncotically active serum proteins results in an expansion of the ECS. The ECS expansion has been demonstrated to lead to a volume fraction increase from 0.19 in normal brain to 0.30.[36] The change in ECS is depicted schematically in **Figure 1-1 B**.

The leaky nature of microvasculature found near tumors may be mainly attributed to abnormalities in tight junctions found between cerebral endothelial cells. Tight junctions are important in maintaining BBB integrity and therefore a disturbance to their structure could lead to conditions of VE. Studies suggest that tumors lead to a deregulation of proteins associated with maintaining the BBB. Liebner *et al.* found a loss of claudin-1 expression in the microvasculature in glioblastoma multiforme and a significant down-regulation of the claudin-5 and occludin tight junctional proteins.[39] Another study also found abnormal expression in occludin associated with tumors.[40]

As stated earlier, BBB integrity is necessary for keeping homeostasis in the brain. In order to study models of VE, it is crucial to understand BBB morphology and how it can be disrupted. These topics are discussed below.

The Blood-Brain Barrier

The brain is separated from systemic circulation by the BBB, which has both a protective and a regulatory role. The BBB is formed by the tight junctions of the endothelial cells that line blood vessels and the astrocytic end feet which surround them.[41]

Astrocytic end feet processes ensheath the microvasculature of the brain and help maintain

the BBB by providing protection against hypoxia and aglycemia.[42] **Figure 2-1** illustrates

differences between capillaries in the brain versus systemic capillaries. Unlike systemic

capillaries, those in the brain lack fenestra, intercellular clefts, and pinocytic vesicles. [8,41]

Furthermore, cerebral endothelial cells contain more mitochondria than non-cerebral

endothelial cells, roughly 3-5 times as much,[8] which are needed by the multiple energy-

dependent transporters in the BBB. In addition to the anatomical barrier created by tight

junctions, studies using iron oxide nanoparticle delivery across the BBB have suggested a

barrier at the level of the basal lamina. [21]

The BBB maintains homeostasis by selectively transporting nutrients into the brain

via several transport mechanisms and structures, including endocytosis, paracellular

diffusion, transcellular diffusion, cation channels, ion antiports, and ion symports.[41]

Receptor mediated endocytosis plays an important role in transporting important molecules

such as iron and insulin, while O_2, CO_2 and lipophilic substances are transported via

transcellular diffusion.[41] Generally, lipid solubility is the most important factor for a

compound to cross the BBB.[8]

The major component of the BBB is the tight junction structure between vascular

endothelial cells. The junctional complex between endothelial cells is comprised of tight

and adherens junctions; tight junctions being the most apical element.[41] Tight junctions are

crucial in maintaining the BBB by limiting the paracellular diffusion of molecules and

inhibiting build up of extracellular fluid.[41] Located in the cholesterol-rich region of the

Figure 2-1: Diagram illustrating differences between cerebral and systemic capillaries. **A**:

Cerebral capillary endothelial cells are sealed together by tight junctions and are surrounded by glial foot processes; this structure forms the blood-brain barrier. **B**: Systemic capillaries have pinocytic vesicles, fenestrations and intercellular clefts, which are not seen in cerebral capillaries. They also exhibit a lower number of mitochondria than cerebral endothelial cells. (Sketch based on diagram by Engelhard and Groothuis[43])
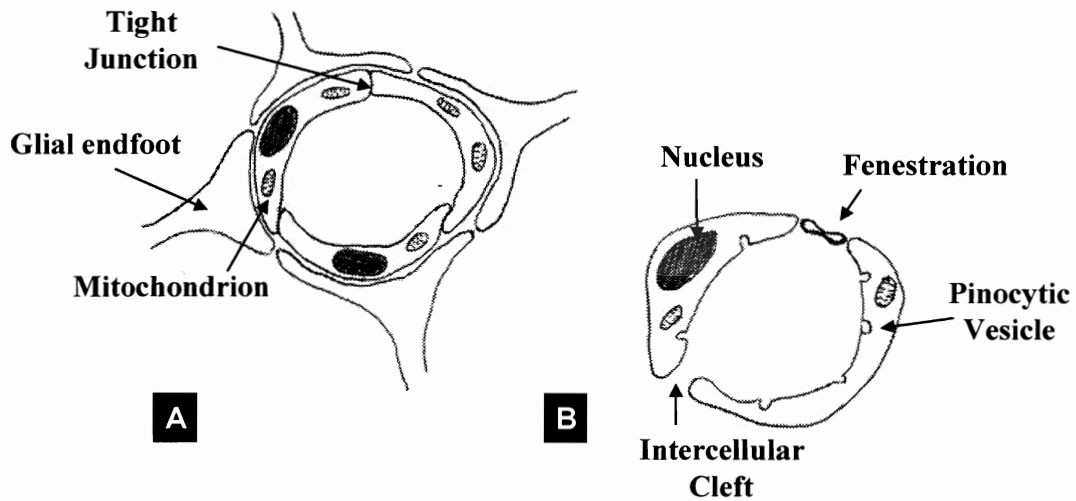
plasma membrane, they are comprised of three integral proteins: (1) claudin, which creates the backbone of tight junctions, forming the primary seal, (2) occludin, which confers increased electrical resistance and decreased paracellular permeability, and (3) junctional adhesion molecules (JAMs) which help regulate leukocyte migration across the BBB.[41] In addition, several accessory proteins are found within tight junctions and provide structural support. These include zona occludens proteins (ZO1, ZO2, ZO3), AF6, 7H6 and cingulin.[41] These transmembrane and cytoplasmic proteins are linked to the actin-based cytoskeleton of the endothelial cells. Actin binds to ZO proteins and studies have shown that actin structural organization can determine tight junction integrity. Substances such as cytokines, cytochalasin D and phalloidin can disrupt actin and have been shown to also disrupt tight junction structure and function.[44;45]

The assembly and disassembly of tight junctions are controlled by intricate signaling cascades involving several cytoplasmic signaling proteins.[41] Extracellular levels of calcium (Ca^{2+}) have been found to play an important role in determining tight junction structure. Ca^{2+} is believed to be involved with the initial events of junctional complex formation,[41] while studies have found that if Ca^{2+} is removed from the extracellular environment, electrical resistance across the membrane is reduced with a concurrent increase in permeability.[46]

The phosphorylation of transmembrane and accessory proteins has been found to be important in regulating tight junction structure. Studies indicate that tyrosine phosphorylation can correlate to decreased occludin expression and increased permeability

across the endothelial cells.[47] As discussed before, the deregulation of these tight

junctional proteins may play a role in forming the tumor related VE.

Tight junction structure is also regulated by endogenous growth factors and

cytokines. Cytokines have been found to increase leukocyte migration,[41] which triggers a

signal transduction cascade that can lead to junctional disorganization via breakdown of

ZO1 and occludin, resulting in blood-brain barrier disruption.[48] Studies have shown that

vasoactive cytokines like TNFα, interleukin 1 β, interferon γ and histamine, in addition to

vascular endothelial growth factor (VEGF) can increase membrane permeability.[49;50]

VEGF is overexpressed in brain tumors, especially in GBM,[8] and is therefore another

mechanism which can lead to conditions promoting VE.

Blood-Brain Barrier Disruption and Clinical Applications

Although protecting the brain from harmful toxins that may appear in systemic

circulation, the BBB does pose a hurdle for delivery of drugs to help pathological brain

states. As discussed above, systemically delivered drugs must overcome issues of

appropriate size, lipid solubility and charge in order to cross into the brain.[21] In fact, the

BBB blocks delivery of over 98% of all drugs.[51]

In order to enhance drug delivery to the brain, techniques in disrupting the BBB

have been explored. Research has shown that bradykinin (BK) can specifically open the

brain-tumor-barriers through a mechanism which is mediated through the B2 receptor on

the endothelial cells.[51] This leads to a transient increase in intracellular Ca^{2+} levels, which

increases nitric oxide synthase (NOS) that results in an increase in the permeability of the microvasculature in brain tumors. [21] The increase in intracellular Ca^{2+} can alter cytoskeletal proteins such as nonmuscle filamin that may also enhance vascular permeability. [21] Understanding this receptor mechanism has led to utilizing a BK analog, RMP-7 (Cereport) clinically as a means of delivering chemotherapeutic agents to brain tumors. [51]

Intra-arterial infusion of mannitol is known for its ability to temporarily open the BBB[52;53] and therefore has been studied as a mechanism for delivery of therapeutic agents to the brain,[54;55] and understanding BBB physiology.[54] Other hypertonic solutions have been used to provide a similar BBB disruption, such as arabinose and saline; however, 1.1M (20%)-1.4M (25%) mannitol is the most commonly used in preclinical and clinical studies, and the most carefully evaluated and proven reversible BBB disruption method.[21] Antineoplastic agents such as methotrexate (MTX) can be harmful in high doses delivered systemically. Hyperosmotic substances such as mannitol are beneficial by increasing delivery of substances like MTX, without the need of increasing the overall systemic dose.[56] In fact, studies have shown that when chemotherapy is administered along with osmotic opening of the BBB, there is up to a 100-fold increase in drug delivery.[21]

In animal studies analyzing BBB disruption, Evan's Blue (EB) dye is the most commonly used agent to indicate osmotic barrier opening. A 2% EB solution is infused intravenously where it tightly binds to albumin. When the dye binds to albumin, the resulting molecule has a molecular weight of 68,500 and therefore does not cross a normal BBB.[21] EB dye can cross over the disrupted BBB in this bound state to mark extravasated

albumin in parenchymal brain tissue, thereby acting as a qualitative indicator of BBB disruption. [54;57]

The current study relies on BBB disruption to create conditions of VE. As discussed briefly above and thoroughly in the next chapter, hyperosmotic mannitol has been well characterized as a BBB disrupting agent and has also been used to create VE. We will examine methods of edema study and various models of VE in the next chapter.

CHAPTER 3

METHODS AND MODELS OF EDEMA STUDY

There are several methods for quantifying the level of edema in brain tissue. Two classical techniques are wet weight/dry weight[58;59] and gravimetric analysis.[60-63] These techniques are discussed below.

Wet Weight/Dry Weight: In this technique, the brain tissue is extracted and dissected in a wet or humid chamber, which ensures preservation of brain water.[64] Brain areas of interest and similar size are excised from the edematous and contralateral symmetrical gray matter.[65] The brain samples are then weighed to obtain a wet weight and then dried to a constant weight at 90-100°C.[65;66] The dry weight is then determined. The percentage of water content is calculated with the following formula: % Water= (1-dry wt/wet wt) x 100%.[65]

Gravimetric: In this technique, the brain is removed and coronal sections are cut. Tissue samples from the desired edematous region are dissected into pieces 1-mm^3 in size.[67-69] Multiple samples from a desired region are removed and placed in kerosene. A layered kerosene-bromobenzene continuous gradient column is utilized for identifying the specific gravity (SPGR) of each sample, and is calibrated with K_2SO_4 samples of known specific gravity. Each sample is placed into the top of the column and allowed to sink and

equilibrate for a period of 1-2 minutes.[70;71] The equilibrium position of the sample within

the column is used to obtain the specific gravity of the wet tissue. These values can be

averaged over the samples from a brain region of interest and converted to water content.[72]

Specific gravity (SPGR) can be converted to grams of water per gram of tissue with an

established equation for rat brain   The following is an example of a formula for cortical

matter in the rat brain: % H_2O/g tissue = (462.6/SPGR) – 362.6.[73] As studied by Fujiwara *et*

al., the specific gravity in gravimetric analysis can be affected by the following four

factors: (1) the purity of monobromobenzene (MBB) and kerosene (K) and, (2) the

temperature (3) duration of interaction of MBB with tissue and/or standard solutions, and

(4) the size of tissue samples.[74]

Gravimetric and wet/dry weight analyses are very invasive procedures that require

time and care for thorough and accurate analysis. Considering the steps these procedures

involve, there is always the possibility of some inaccuracies due to water loss in the brain

between extraction, slicing and edema measurements. The use of MRI is a non-invasive in

method that provides a high sensitivity of relaxation times of water content changes.[75]

Therefore, MRI is a useful tool for in vivo brain edema analysis[76;77] The current study will

track and analyze edema development by utilizing several MRI modalities: T2 imaging,

water maps, and ADC maps.

T2-weighted imaging is useful for identifying brain edema, due to its sensitivity to

increase in water content in the brain, and has been utilized in many edema studies.[55;78]

The dynamic structure and amount of brain tissue water directly influences T2 relaxation

times.[79] T2-weighted images provide a qualitative assessment of increased water content,

which appears as hyperintense regions in the image.[80] MRI can also be used for obtaining

quantitative data by way of ADC and water map analysis.

Water Maps: Water maps provide a quantitative assessment of the brain tissue water

content, or water fraction (f_w). These water maps are generated from T1 maps, where

relaxation times are sensitive to changes in water content.[81] Fatouros, *et al.* first developed

an accurate in vivo model for f_w assessment based on a fast exchange two-state model,

which was validated by phantom and animal brain edema models, and later verified with

human study.[82] "Free" bulk water in the brain exhibits long relaxation time, while

restricted ("bound") water, which is hydrogen-bonded to macromolecules in hydration

layers, has shorter relaxation times.[83] The longitudinal T1 relaxation time is a weighted

average between the "free" and "bound" water.[84] To acquire a pure T1 image, sequential

inversion recovery images are processed, and then the T1 map points are converted to

water fraction values.[85] These values appear in a water map that can be analyzed by

computer software in which regions of interest (ROI) can be evaluated. Normal human

brain water was measured to range from 68% to 80% depending on the tissue type and

region.[86] Brain water analysis via this technique has correlated well with the gravimetric

results (R^2=0.976),[87] thereby validating this as an accurate and non-invasive technique.

Both T2 weighted imaging and water fraction analysis provide techniques for

identifying and measuring edema in the brain, respectively. However, for the purposes of

the current study, it is vital to be able to characterize the type of edema that is present. One

proven technique for this is ADC map analysis.

ADC Maps: ADC maps are processed from a series of diffusion-weighted images (DWI) acquired at varying magnetic fields.[9] This imaging is sensitive to the diffusion of brain water.[88] ADC values represent a quantification of water movement that can be affected by many factors such as passive Brownian thermal diffusion, active transport, and bulk movement.[89] Water can be restricted by cell membranes[90] and macromolecular binding.[91] Thus, water in both ECS and intracellular space (ICS) is subject to different types of, and barriers to, motion.[92] Faster diffusing water found in the ECS would provide higher ADC values, and therefore VE is characterized by an increase in ADC values.[9] However, ADC values decrease in conditions of CE, due to increased ICS water, which is less mobile, due to interaction with intracellular macromolcules.[9] Using a MCA occlusion model for CE, Ito et al., demonstrated an ADC decrease in the rat brain from baseline of 0.6×10^{-3} mm^2/sec to near 0.4×10^{-3} mm^2/sec.[9] Using a direct infusion model of VE, ADC values climbed to above 1.4 mm^2/sec within an hour after cessation of infusion.[9] Examining changes in ADC values in conjunction with T2 images provides a useful technique for evaluating the presence of VE or CE. Studies have used this to verify the presence of particular edema type in humans, with VE being indicated by elevated ADC and hyperintense T2 changes.[93]

The aforementioned MRI modalities will be utilized in the assessment of our VE model's characteristics and applicability to CED study. In order to select a model of VE, published models of VE were examined for their applicability for rat brain-based CED studies. A review of these models is presented next.

Models of Vasogenic Edema

Various animal models of VE have been used by researchers, such as albumin injection [94], cold-injury[94-96], and unsaturated fatty acid emulsion,[97] and intra-arterial mannitol infusion.[55] Below is a survey of some of these models and their applicability to the current study. Some techniques discussed below were introduced in the previous chapter's discussion of BBB disruption. The current study was in need of a rat-based model that would demonstrate repeatable conditions of VE in brain regions applicable for Gd-DTPA infusion and homogenous distribution such as deep gray striatum or cortical gray region of the forebrain.

Infusion VE Model

While a number of models of this type of ECS alteration have been developed, one of the simplest and most reliable is the infusion of a solution of normal saline containing serum albumin.[98-102] This infusion model involves intraparenchymal infusion of albumin mixed with mock CSF via a stereotactically placed cannula into the area of interest such as white matter or striatum.[103] This results in expansion of the ECS in a manner analogous to that seen in human brain,[104] which reaches a maximum over approximately 24 hours, and can persist for multiple days before resolving.[102;105;106] The infusion edema model for VE shows increased water diffusion in the ECS as evidenced by hyperintense regions on ADC maps;[3] Ito *et al.* demonstrated that ADC values increase within an hour of infusion.[9]

Studies conducted by Haar *et al.* utilized this model to investigate CED under conditions of VE.[3] His study involved direct infusion of albumin into parenchymal tissue along a tract made 1mm anterior to the subsequent site for the infusion cannula tract. Gd-DTPA was utilized as a model therapeutic agent for CED.[3] As mentioned in the first chapter, these studies proved inconclusive for studying VE in the rat brain. Reasons for this were listed as primarily due to the invasive nature of the model possibly creating some CE, the small size of the brain and additional factors such as tissue impedance, pore fluid pressure and the interactions between the tissue and cannula.[3] The small size of the rat brain meant that the Gd-DTPA cannula tract was close in proximity to the albumin infusion tract and white matter, thereby potentially affecting the results. Since the current study is to be conducted in the rat brain, the model for VE should be as minimally invasive as possible with respect to the brain parenchyma, in order to study CED in tissue that has not been altered in any way, apart from the edema itself. To avoid the experimental limitations observed by Haar, the albumin infusion model was abandoned and other VE models were explored for CED study.

Unsaturated Fatty Acid Model

The unsaturated fatty acid emulsion model is a novel technique which has produced VE in the cat brain.[97] The fat emulsion was made via a mixture of linoleic acid or oleic acid with saline. The fat globules formed were less than 2 times the size of red blood cells.[97] This emulsion was infused cephalad into the internal carotid artery for 5 minutes at a rate of 4mL/min.[97] This model may have some potential when used for research with

BBB disruption. MRI studies revealed VE and reversible changes after the unsaturated fatty acid emulsion was infused into the carotid artery. Specifically, diffusion-weighted imaging (DWI) and subsequent ADC maps showed evidence of VE 1 hour after emulsion infusion and no sign of cytotoxic effect.[97] Although this may be useful, no studies are available to prove the effectiveness of this technique in the rat brain, nor have consistent areas of large edematous regions in the gray matter been demonstrated.

Toxin-induced Model

Another method of inducing conditions of VE in the rat is intraperitoneal injection of a toxin. One study has explored this model using Hooded Wistar rats injected with the *Clostridium Perfringens (Cl P)* type D epsilon toxin which preferentially binds to the brain.[107] Although the mechanism that causes the VE to form is unknown, the authors used immunocytochemistry to detect the presence of endogenous albumin.[107] They found albumin in the walls of the cerebral microvessels as soon as 1 hour post injection, with maximal leakage of albumin into the parenchyma occurring at 24 and 48 hours.[107] The authors found a partial reduction in expression of endothelial barrier antigen (EBA) that was most prominent at 24 and 48 hours post-injection of the toxin.[107] EBA is a protein with barrier function and is specifically expressed by rat CNS endothelial cells. Immunostaining for EBA can also be used to detect BBB disruption.[107] Although this toxin-based model seems to produce VE conditions, the breadth of such edema development has not been characterized or shown to be repeatable in specific regions of the rat brain.

Another toxin model for VE has been produced in piglets using an intrathecal injection of bacterial lipopolysaccharide (LPS).[108] Clinical conditions such as bacterial meningitis and traumatic brain injury show an increase in BBB permeability that is mediated by inflammatory reaction. LPS from *E. coli* was used to mimic such inflammatory conditions to produce VE. The LPS was injected into the cisterna magna while the intracranial pressure (ICP) and cerebral blood flow (CBF) were measured, along with intracerebral microdialysis to analyze interstitial levels of glucose, pyruvate, lactate, glutamate, glycerol and urea.[108] The authors found that 4-7 hours post LPS injection, ICP increased and reached a plateau, and CBF increased by 46%. The LPS caused a statistically significant decrease in glucose and increase in lactate/pyruvate ratio. There was no increase in glycerol, leading the authors to conclude that there were no biochemical signs of cell membrane degradation or tissue damage. This model, however, has not been tested or characterized in the rat brain, like the unsaturated fatty acid model discussed previously.

Cold Injury Model

Another widely used model for VE is the cold-lesion or cold-injury model.[109] This is commonly created by application of a cooled metal probe to either an intact cranium or dura. The metal probe can range from aluminum[110] to copper[111] and is cooled to temperatures around –80°C in a mixture of dry ice and methyl butane,[112] or liquid nitrogen.[113] It is then placed onto the dura mater over the left parietal cortex for 30 seconds through a 5-mm-wide craniotomy.[114]

The cold-injury produces a necrotic lesion mainly confined to the cortical gray matter surrounded by a narrow zone of increased permeability.[115] MRI studies of the cold injury model have shown a periphery region of VE surrounding the area of insult.[116] The resulting edema does not form from the lesion area itself since the vessels in the lesion area are rapidly occluded by intravascular thrombosis.[117] The likely method of extravasation in the area below the lesion is pinocytic activity as suggested by Baker *et al*.[118] Another study mentions that removal of necrotic tissue will prevent formation of edema, thus suggesting that a substance released from the necrotic tissue is a stimulus for pinocytosis. As edema fluid spreads from this region, it moves into adjacent white matter via bulk flow.[119]

After cold-injury, cortical necrosis peaks after 24 hours,[120] with maximal BBB disruption 24 hours after injury.[121] The delayed build-up of edema is attributed to oxygen free radicals, as seen in cortical brain injury and traumatic brain injury.[122] During this time, the volume of the lesion can expand up to 400%, which can be attributed to the progressive death of parenchymal tissue and is an important manifestation of secondary brain damage. This injury is further complicated by development of VE. One study has shown that the freeze injury induced brain edema can decrease the microcirculatory blood flow up to 50% from baseline. This results from the narrowing of the capillaries due to compression by swollen astrocytic processes.[123] The posttraumatic hemispheric swelling reaches 50% of its maximum at 1 hour and maximum at 12 hours.

A wet-dry weight analysis of the brains post cold-injury showed a peak water value of 79.87% after 2 hours, which then gradually decreased and fell after 32 hours to below the control value of $78.22 \pm 0.47\%$.[124] Excess protein content in the injured hemisphere

peaked at a value of 21.54±2.76 mg/g dry weight after 8 hours. The uninjured hemisphere was considered to have a negligible level of protein extravasation, which was by definition, zero.[125]

The cold-injury model can produce conditions of VE in a peripheral region of injury,[126] but is not applicable for CED studies due to the shape and cortical localization of the edema. The region of edema does not penetrate into the deeper gray matter of the brain nor does it create an expansive volume of edema that can be used for studying Gd-DTPA CED. The current study required the brain volume of edema to be more widespread and larger than the planned infusate distribution. Creating a widespread region of edema within a hemisphere is important for studying how the infusate will behave under conditions of VE. It was also necessary to have conditions of parenchymal space enlargement as seen in VE and not a combination of other injury as seen in cold-injury.[127] The perturbation itself may alter the tissue in an unpredictable or irreproducible manner, in addition to the associated brain necrosis that may complicate the infusion studies. For these reasons, the cold-injury model was not selected for the current study.

Mannitol Model

Studies have found that intracarotid injection of 25% (1.4M) mannitol can create reversible opening of the BBB by inducing cerebrovascular dilation and osmotic cell shrinkage of endothelial cells. This allows for the widening of the interendothelial tight junctions to an estimated radius of 200Å.[21;53;128] At the subcellular level, there may be second messenger systems (e.g. calcium influx and nitric oxide) effected by osmotic stress

along with cytoskeletal changes, all contributing to the barrier opening.[21] Studies have

shown that this opening is reversible, with vascular permeability returned to baseline

within 24 ± 14.3 minutes.[21]

As mentioned in previous chapters, intra-arterial infusion of mannitol is utilized in

the clinical setting to open the BBB for drug delivery.[129] Mannitol is also clinically

administered via intravenous (IV) infusion in order to lower intracranial pressure (ICP)

after development of edema.[130-133] IV delivery of mannitol can reduce ICP by acutely

lowering blood viscosity and increasing cerebral blood flow, which triggers cerebral

arterioles to undergo autoregulatory vasoconstriction.[134] This autoregulatory mechanism

directly affects cerebral blood flow, thus controlling the volume of intracranial blood and

thereby lowering the ICP.[135]

Animal researchers deliver mannitol to the brain by way of internal carotid artery

(ICA) utilizing two different catheterization techniques. Some experiments have involved

retrograde catheterization of the external carotid artery (ECA) with SP-10 tubing to the

bifurcation of ECA and ICA with ligation of the pterygopalatine artery (PTA). [57;95;136-138]

Other studies directly catheterize via the common carotid artery using PE-50 tubing while

ligating the proximal end of the external carotid and pterygopalatine arteries.[57;139] Animal

subjects are anesthetized via isoflurane while the degree of BBB disruption can be

monitored by EB dye delivered via femoral vein prior to mannitol infusion.[54]

Kaya et al. observed the following effects after left ICA infusion of mannitol: (1)

cardiovascular depression during infusion leading to a drop in arterial blood pressure,

returning to normal values within seconds of infusion, (2) water content in the left

hemisphere of the brain increased significantly compared to the right hemisphere within 10 minutes of infusion, and (3) BBB permeability to albumin, as seen by EB staining, was significant in the left hemisphere.[57] The same study found that magnesium sulfate, when delivered via intracarotid or intraperitonial routes, can attenuate the BBB disruption effect of mannitol.[57]

A previous study has shown that for the highest amount of BBB disruption with reduced mortality, an optimal rate of infusion of 25% mannitol at 37°C for adult Sprague-Dawley rats is 0.25ml/kg/s over 30 seconds.[95] This rate and duration can lead to a reliable, reversible BBB opening without an immediate or delayed neurotoxic effects.[57;95] Studies have found that this concentration of mannitol has shown excellent BBB disruption in 95% of normal rats.[21] For a 300g rat, this amounts to a flow rate of roughly 4.5 ml/min and a total amount of 2.25ml of solution delivered.

Histological rat brain studies by Salahuddin et al. have shown that after one hour, a single 1.5mL injection of 1.4M (25%) mannitol via the ICA can lead to spongy appearance in the neuropil, perivascular swelling and collapsed, dark neurons.[136;137] These pyknotic cells can be considered either dead or dying which will eventually be subject to macrophage mediated removal.[136] Further investigation using electron microscopy has yielded that the dark and shrunken neurons were collapsed and surrounded by swollen processes which were mostly astrocytic origin.[137] The perivascular swelling was found to be due to swollen astrocytic processes as well.[137] The spongy appearance in the neuropil was also attributed to swollen cellular processes.[137] The shrunken cellular appearance was attributed by the authors to possible CE.[137] However, the same study does cite VE being

observed.[137] Although that study was not clear as to how VE was observed, other literature has listed swollen astrocytic processes and perivascular end feet as indications of VE.[140] Dilated spaces around capillaries have been observed in other VE studies.[141] These astrocytes are believed to swell due to pinocytosis of fluid from escaped vessels.[142]

As reviewed in this chapter, BBB disruption due to mannitol infusion has been investigated in many studies;[57;136;137;143] however, based on a database search, only one study actually utilized mannitol specifically for creation VE, via multiple mannitol infusion in the internal carotid artery of mongrel dogs.[55]

Based on the mannitol effects illustrated by Kaya *et al.*[57] and previous use by Turski *et al.*,[55] it appeared that favorable conditions of VE could be achieved with mannitol induced BBB disruption. Of all the researched models, mannitol delivery seems the most applicable for infusion studies. Intra-arterial infusion of mannitol appears to have the possibility of creating a wide-spread area of edema in the deep and cortical gray matter, without any other complications (e.g. brain necrosis seen with the cold-injury model[55]).

The current study will focus on using mannitol infusion to model conditions of pure VE in the rat brain. Although the time course of BBB disruption has been extensively studied[95;137] the characterization of edema in the rat brain induced by intraarterial delivery of mannitol has not been reported. The current study will characterize the time course and extent of edema formation in order to establish a model of VE suitable for CED studies.

CHAPTER 4

HYPOTHESIS AND SPECIFIC AIMS

In order to plan effective targeted convective drug delivery into the brain, it is important to understand how the infusate will distribute in the pathological tissue. For example, chemotherapeutic treatment of brain tumors requires knowledge of how the agent infused via CED will distribute in brain tissue exhibiting VE seen in peritumoral regions. Although CED has been characterized in normal brain and conditions of CE, there has been little success in obtaining conclusive results under conditions of VE.[3] Previous studies conducted by Haar utilized direct parenchymal infusion of albumin to create a model of VE.[3] This model, however, proved incompatible with CED study and therefore a new model was needed. The purpose of the current study was to modify an existing model of VE in order to create conditions of VE in a consistent and reliable fashion that will cover an area large enough to contain the volume of CED infusate.

Background research on current models of VE, as reviewed in the previous chapter, led to the possibility of using intracarotid infusions of 25% mannitol. Utilizing the knowledge of previous studies that employed mannitol for BBB disruption and VE production, the current study tested different doses of mannitol to achieve optimal conditions of VE. MRI techniques and histological examination were used to verify the

presence of VE and characterize the time-course of edema development to determine its applicability for future Gd-DTPA CED studies.

Hypothesis: Multiple intracarotid infusions of 25% mannitol will create reproducible conditions of pure VE in the gray matter of a single hemisphere in the rat brain. The tissue volume affected by VE will be larger than a planned model therapeutic CED infusate volume and the time course of VE long enough for infusate to distribute and be measured.

Specific Aims:

1) To use multiple infusions of mannitol to obtain reproducible and unilateral edema for CED study in the gray matter of the rat brain.

2) To characterize the time course of edema development.

3) To verify presence of VE with T2 imaging, ADC value analysis, water maps and histological analysis.

CHAPTER 5

METHODS

All animal experiments were approved by the Committee for the Care and Use of Laboratory Animals at Virginia Commonwealth University. Male Sprague-Dawley rats with an average weight of 320g were anesthetized and catheterized via the right common carotid artery (CCA) and femoral vein. Preliminary experiments were conducted (n= 17) in which mannitol was infused at different rates and volumes until a consistent and unilateral edema was observed based on EB dye staining and T2-weighted MRI.

From these studies, we found that 3 infusions of 25% mannitol 30 minutes apart could possibly serve as a viable model for VE in the rat brain, which warranted further investigation. Rats (n=11) received this series of mannitol infusion and after the third infusion, MRI was conducted 30 minutes, 1 hour, 24 hours and 48 hours later. Control rats (n=9) were left untreated and scanned. Sham operated animals (n=4) were operated and scanned at 1 hour (n=2) and 48 hours (n=2). For histological studies, 3 rats with 3 infusions of mannitol were sacrificed 2 hours after the last infusion. Further rats were processed for control (n=2), which were left untreated, and sham-operated animals sacrificed 2 hours (n=1), and 48 hours (n=1) after CCA ligation. Details for the procedures, imaging, histological processing and data analysis are discussed below.

Mannitol Infusion Model

CCA Catheterization: (**Figure 5-1 A)** Rats were anesthetized with 1.5% isoflurane in a 2:1

mixture of nitrous oxide and oxygen, and rectal temperature was maintained at 37°C using

a heat pad. Through a midline neck incision, the right CCA was exposed along with the

internal carotid artery (ICA) and external carotid artery (ECA) branches. The occipital

artery was cauterized and dissected to expose the ICA branch. A 4-0 suture was used to

ligate the ECA, while a 6-0 suture was used to ligate the pterygopalatine artery (PTA)

branch of the ICA. This ligating of arterial branches ensured mannitol infusion would only

occur along the ICA into the right hemisphere of the brain. The CCA was ligated at the

proximal end and a P-50 catheter was introduced into the lumen and inserted up through

the ICA origin. The catheter was secured by tightening another 4-0 suture around the

catheterized CCA. The femoral vein was also catheterized in a similar fashion with a P-50

catheter, after ligating the distal end with a 4-0 suture.

Femoral Vein Catheterization: (**Figure 5-1 B)** The right femoral vein was exposed and

ligated with a 4-0 suture at the distal end. A PE-50 catheter was inserted into the right

femoral artery for either blood pressure monitoring (n=5), or EB dye delivery (n=5).

Figure 5-1. Diagram depicting catheterization of CCA and femoral vein. **A:** The CCA with catheter and ligated branches (the occipital artery is cauterized). **B:** The femoral vein catheterized and ligated.
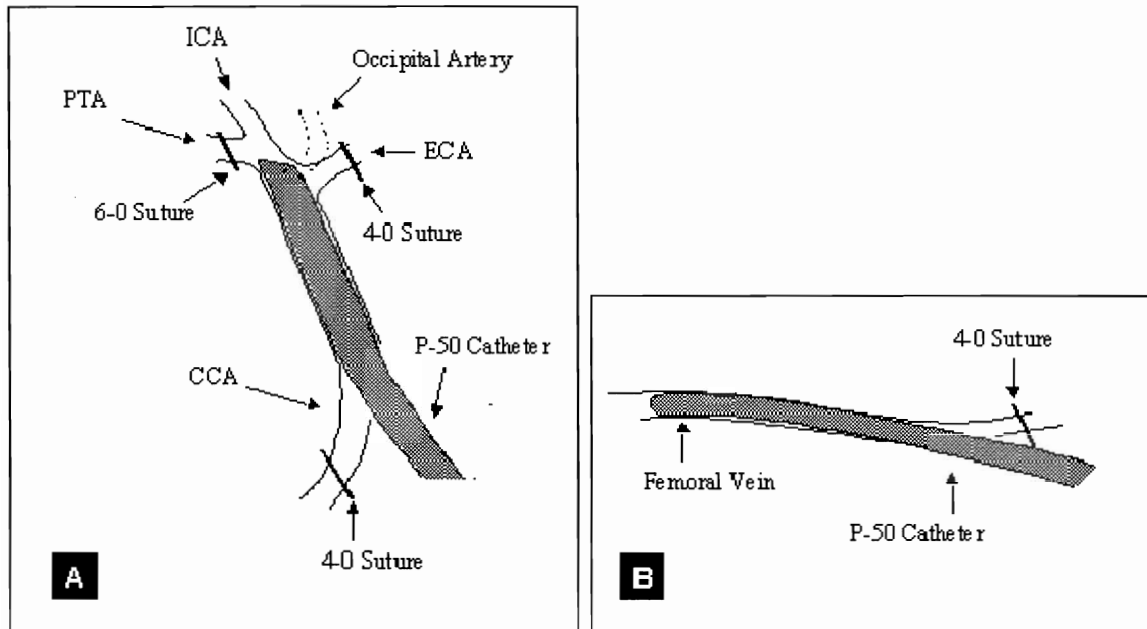
Evan's Blue Dye: EB dye was utilized to mark BBB disruption on mannitol infused rats

(n=5), and brains were examined 2 hours (n=3) and 48 hours (n=2) after the last mannitol

infusion. EB dye (2% in saline) was delivered at 2ml/kg via the catheterized femoral vein

5 minutes prior to the first mannitol infusion.

Mannitol: Mannitol (25% at 37.0±1°C) was delivered via catheterized CCA at 2.5ml/kg/s

for a period of 30 seconds. In total, 3 doses of mannitol were delivered at 30-minute

intervals. After the third infusion, the catheters were removed.

Imaging: Control rats (n=9) were left untreated for imaging. For surgical control, sham-

operated rats (n=4) had their right CCA sutured closed and were imaged 1 hour (n=2) or 48

hours later (n=2). Mannitol was infused in 11 rats. After the third mannitol infusion, rats

were scanned to acquire T2-weighted (T2W), diffusion-weighted (DWI), and T1 Maps

(T1M). The time interval between the infusion and imaging and rats scanned per image

type were as follows: 30 minutes (n=3 for DWI and T1M), 1 hour (n=4 for DWI and

T1M), 24 hours (n=2 for DWI, n=3 for T1M) and 48 hours (n=3 for DWI, n=4 for T1M).

Although EPI DWI imaging was used for its short acquisition time, some the same rats

(n=5) were also imaged with SE DWI for control (n=1), after 1 hour (n=2), and after 1.5

hours (n=3) of mannitol infusion. T2 images were acquired at every scan. Imaging

procedures are described below.

Imaging placement: Each rat to be scanned was either kept under isoflurane anesthesia if imaging was conducted on the same day as mannitol infusion, or anesthetized by intraperitonial administration of 0.5 ml of ketamine (50mg/ml) for 24 and 48-hour follow-up. Each rat was placed in an acrylic imaging tube, secured via plastic ear bars, and fitted with a surface coil. Images were acquired with a 2.4 T, 40-cm bore magnet (Bruker Medical, Inc., Billerica, MA) equipped with a 12 cm inner-diameter, actively shielded gradient insert (maximum gradient strength: 25 G/cm). An actively decoupled RF coil set was used for RF excitation/reception and was comprised of a 7 cm inner-diameter "birdcage" design resonator and a 2 cm diameter circular surface coil.

T2 images: T2-weighted images with echo time (TE) of 100 msec, and repetition time (TR) of 3000 msec, were obtained on 7 contiguous coronal slices 2-mm thick with a resolution of 96 by 96.

EPI DWI: DWI (TR: 1500 msec/ TE: 41msec) images were taken which employed an echo planar based spin echo sequence appropriately modified to include diffusion-sensitizing gradients along the readout (horizontal) direction with a duration of 9msec and a gradient separation of 20 msec. Each data set consisted of 5 coronal slices of the forebrain and midbrain region, each slice being 2-mm thick with a resolution of 128 by 128 and a 30-mm^2 field of view. Diffusion weighting factors, or b values of 0 and 1042s/mm^2 were used (maximum gradient strength of 23 G/cm). ADC maps were processed from DWI images using the MRVision software package (MRVision Co., Winchester, MA).

SE DWI: DWI (TR: 1500 msec/ TE: 39 msec) images were taken which employed a spin echo sequence appropriately modified to include diffusion-sensitizing gradients along the readout (horizontal) direction with a duration of 4 msec and a gradient separation of 25 msec. Each data set consisted of 5 coronal slices of the forebrain and midbrain region, each slice being 2-mm thick with a resolution of 128 by 128 and a 30-mm^2 field of view. Diffusion weighting factors, or b values of 4.2, 160.5, 557.6, and 1195.6 s/mm^2 were used (maximum gradient strength of 23 G/cm). ADC maps were processed from DWI images using the MRVision software package (MRVision Co., Winchester, MA).

T1 images: Two-dimensional T1 imaging series were generated with a spin echo, echo-planar imaging sequence preceded by an inversion recovery preparation period using a hyperbolic secant inversion pulse. T1 maps were calculated from data obtained on 4 coronal sections at a thickness of 2.5mm and slice separation of 3.0mm. Inversion recovery times were: 30, 60, 150, 300, 700, 1300, and 2500 msec.

Data Analysis: Average ADC values were obtained from regions-of-interest (ROI) outlined in the cortical and deep gray matter over four slices. Water maps were calculated from the T1 Maps using the MRVision software. Average water fraction (f_w) values are extracted from ROIs defined in cortical and deep gray tissue structures over four slices. **Figure 5-2** provides an example of left hemisphere cortical and deep gray ROI outlines examined on ADC and water maps, similar ROIs were used on the right hemisphere. Mean

ADC and f_w values from edematous regions for each time period were compared to

contralateral and untreated brain means using t-tests and graphical analysis.

Gd-DTPA infusion

These steps were carried out to test the appearance of infusate in a selected region

of the brain such that volume of distribution would occupy edematous tissue. Utilizing T2

images from preliminary experiments, a tentative CED infusion sight located in the cortical

gray of the forebrain (4 mm anterior and 3 mm right lateral to bregma). The

macromolecular contrast agent gadolinium (Gd) chelated by diethylenetriamine pentaacetic

acid (DTPA), (Gd-DTPA), was utilized to model therapeutic agent distribution.

Guide cannula implantation: 2 rats received a fixed guide cannula 24 hours prior to

imaging as follows. Each rat was anesthetized by intraperitoneal administration of 0.5 ml

of 1:10 ketamine:xylazene mixture (both 50mg/ml) and positioned in a stereotactic frame.

Based on preliminary mannitol studies, a location in the right frontal cortex was decided

upon as an infusion site. An infusion burr hole was created 3 mm lateral and 4 mm anterior

to bregma. An outer guide cannula (Plastics One, Inc.; Roanoke, VA) was stereotactically

placed through the infusion burr hole and fixed to the skull and to a plastic anchor screw

using methylmethacrylate. The tip of the guide cannula was capped until infusion.

Figure 5-2. Example ROIs outlined on ADC and Water Maps. **A**: ROIs drawn in left cortical and deep gray on an ADC map. **B**: ROIs drawn in left cortical and deep gray on a water map.
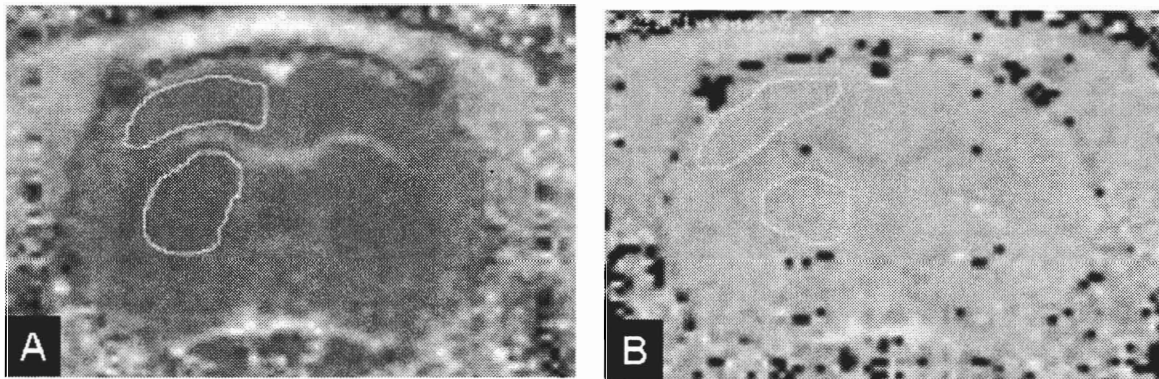
Contrast infusion and imaging: Rats (n=2) received identical infusions of 10.833 mM Gd-DTPA in mock CSF. This solution was doped with 0.11mM manganese chloride to match the T1 value of the rat caudate putamen. The rat was positioned inside an acrylic imaging tube, secured with plastic ear bars, and fitted with the circular surface coil (Bruker, Billerica, MA). An inner cannula was inserted into the infusion guide cannula, the rat and entire acrylic imaging tube placed in the magnet, and 10 µl of the Gd-DTPA solution was infused at a steady rate of 0.2 µl/minute over 50 minutes, using a motor-driven syringe (Bioanalytical Systems, Inc., West Lafayette, IN). During and following this infusion, T1 mapping data was acquired every 10 minutes for 130 minutes, resulting in 13 data sets. T1 maps were calculated from data obtained on 4 coronal sections at a thickness of 2.5mm and slice separation of 3.0mm. Inversion recovery times were: 30, 60, 150, 300, 700, 1300, and 2500 msec. Each rat was then removed from the magnet and sacrificed.

Histological Procedures

Common Preparation for Light and Electron Microscopy: Untreated, sham-operated and mannitol-infused rats were prepared for both light (LM) and transmission electron microscopy (TEM). 2 hours post mannitol infusion, rats were transcardially perfused via catheter inserted into the left ventricle. First, 0.9% saline was delivered for 2-3 minutes until the returning perfusate from the right atrium appeared cleared of blood. Next, perfusion of fixative was initiated. Fixative was a solution of 4% paraformaldehyde and 2% glutaraldehyde in 0.1M Sorenson's phosphate buffer. A total of 500mL of fixative was perfused through the brain. The brain was extracted and sectioned into 4 coronal slices,

beginning from the frontal pole at the following thickness: 3mm, 2mm, 3mm, and 3mm. The 2mm slices were processed for TEM analysis and remaining tissue was utilized for LM processing.

Light Microscopy Preparation: Each slice for LM study was embedded in paraffin blocks. From each block, 2 consecutive 7 μm slices were cut with a microtome. Each slice was re-hydrated with graded ethanol series: 100%, 90%, and 70% for two minutes each. Next they were stained with hematoxylin then with eosin stains. After staining, each slice was dehydrated with graded ethanol and 2 consecutive slices from the same block were mounted on the same slide with permount. Images were captured using the Nikon E800 M Eclipse Microscope with SpotRT camera (Diagnostic Instruments).

Transmission Electron Microscopy Preparation: The 2-mm thick sample for EM study was cut via vibratome into 3 consecutive 40 μm thick slices, with remaining tissue processed for LM study. Each slice from the sample was washed with 0.1M Sorensen's phosphate buffer at 4°C then postfixed with 1% osmium tetroxide in 0.1M phosphate buffer at 4°C for 1 hour. Samples were then washed with buffer and dehydrated with a cold ethanol series: 50%, 70%, 80%, and 95%, for 5 minutes each. Next, slices were dehydrated with 100% ethanol at 20°C, followed by 3 changes of 100% propylene oxide for 10 minutes each. Slices were placed in a 1:1 propylene oxide:PolyBed solution for 4 hours, and then transferred to pure PolyBed resin overnight. Each section was embedded on vinyl slides and placed in a 60°C oven overnight. After LM examination, sections were chosen and

excised from the cortical and deep gray region for remounting on blocks and further

sectioning. Using the LKB 2120 Ultramicrotome, 900Å sections were cut with a diamond

knife. Each section was then placed on Formvar-coated slotted grids and stained with

uranyl acetate and lead citrate for TEM study. A JEOL JEM-1230 (JEOL USA, Inc.)

transmission electron microscope was used to capture images via the Ultrascan 4000

camera (Gatan, Inc.)

CHAPTER 5

RESULTS

The selected mannitol model for VE involved 3 doses of right intracarotid mannitol

infusion at a rate of 0.25ml/kg/sec over 30 seconds, 30 minutes apart. This model was

examined by qualitative and quantitative analysis of data obtained from MRI, gross and

histological tissue examination. Gross brain observation using EB dye was conducted to

look for evidence of BBB disruption. MRI was used to track development of edema over

time using water (f_w) map and ADC map analysis. T2-weighted imaging provided a

qualitative understanding of edema development. Light microscopy (LM) and

transmission electron microscopy (TEM) were used to examine the treatment effect on the

tissue and support evidence of any edematous conditions discerned from MRI study. The

results from each of these analyses are described below.

Evan's Blue Dye

Brains extracted from rats after mannitol delivery clearly showed unilateral EB dye

staining in the right hemisphere. **Figure 6-1** shows a representative image of the brain

upon extraction 2 hours after the 3rd mannitol infusion. All rats that had brains perfused

with mannitol into the right internal carotid artery (ICA) exhibited staining throughout the

ipsilateral hemisphere. As seen in the coronal sections, the staining permeated through the

cortical and deep gray (caudate/putamen) matter, while the contralateral left hemisphere

remained unstained.

T2-Weighted Images

The T2W images obtained 30 minutes and 1 hour after the last mannitol infusion

displayed a consistent and marked hyperintensity through the right hemisphere, ipsilateral

to infusion. This was a unilateral hyperintensity that appears to occur through all of the

forebrain and midbrain cortical and majority of deep gray (caudate/putamen) regions.

Swelling was also observed within the right hemisphere, marked by a midline shift. There

was no apparent hyperintensity in the contralateral gray matter, however, the contralateral

ventricles and white matter did show some hyperintensity. Similar results were seen in the

T2W images 1 hour after the last mannitol infusion. **Figure 6-2 A** contains T2W images of

a sham-operated and a normal untreated control rat brain, both exhibiting uniform intensity

throughout the hemispheric gray and white matter. **Figure 6-3 A** and **Figure 6-4 A** depict

representative T2W images of a brain after 30 minutes and 1 hour, respectively, from

different animals. An untreated rat brain T2W image is included for comparison. **Figure

6-5 A** and **Figure 6-6 A** respectively depict T2W images from the same rat after 24 and 48

hours of infusion and include an untreated rat brain T2W image for comparison. T2W

images seen after 24 hours displayed a large reduction in swelling and hyperintensity when

compared to the previous day scans, with some remaining hyperintensity in the cortical

gray region of the forebrain. After 48 hours, the T2W images displayed no obvious

swelling. In addition, with the exception of some reduction in the right cortical hyperintensity seen 24 hours prior, the right hemisphere gray matter intensity appeared to match controls.

Figure 6-1. Photograph of brain extracted 2 hours after last mannitol infusion. Note unilateral right hemisphere staining by Evan's Blue dye.
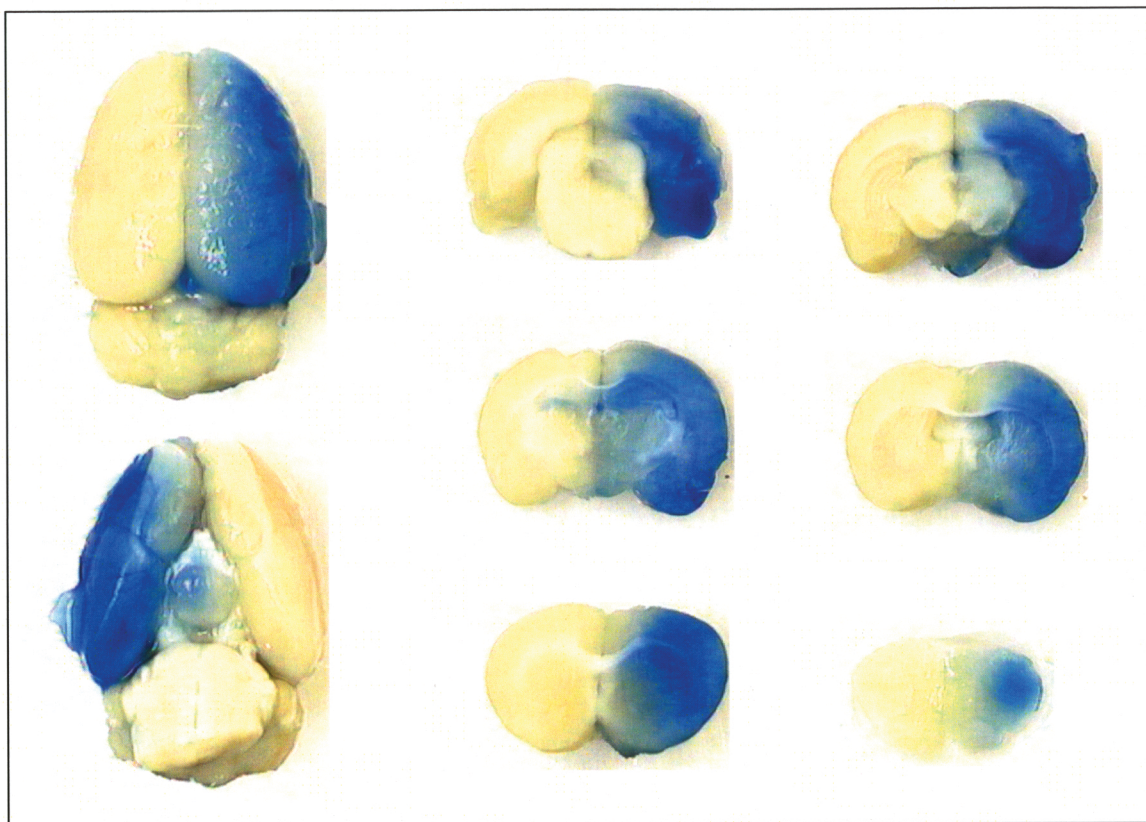
Figure 6-2: T2-weighted image of sham-operated and untreated control rat brain. **A**: Sham-operated animal 2 hours after surgery. **B**: Untreated control rat brain
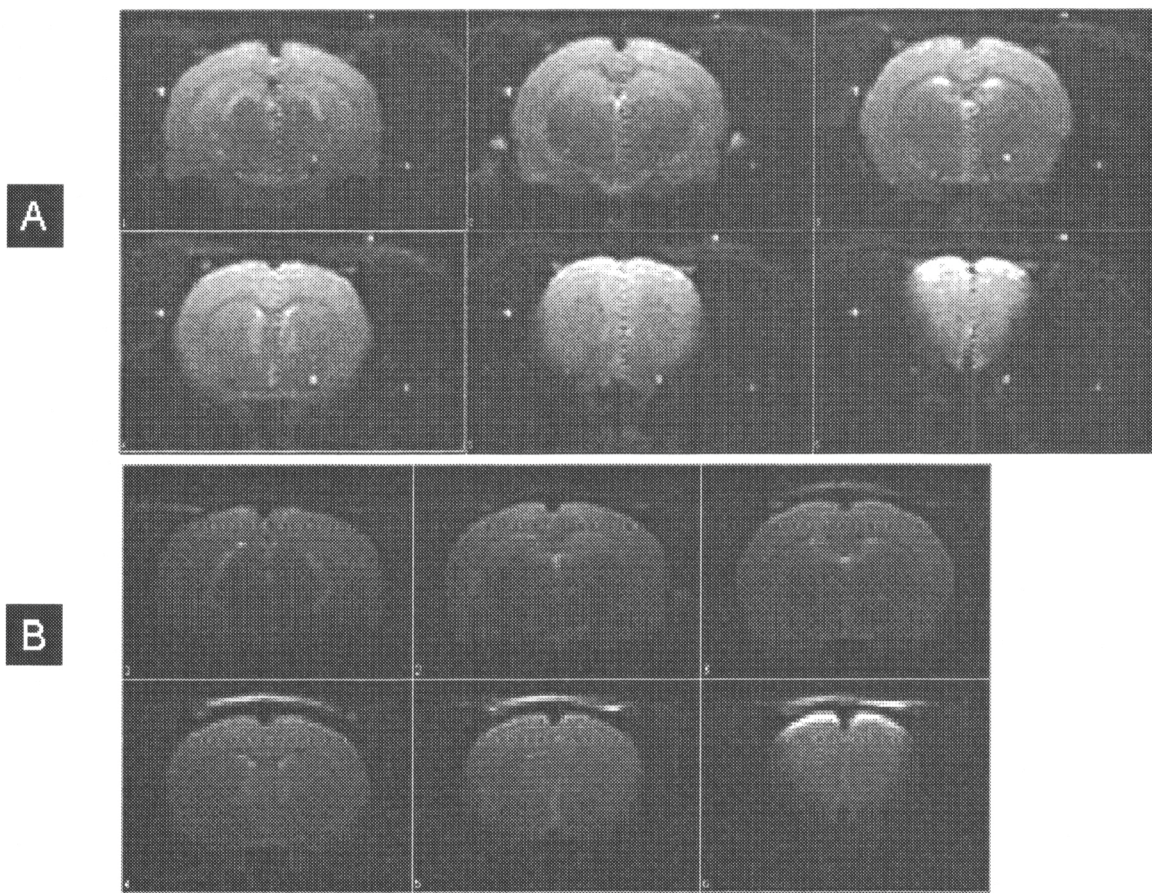
Figure 6-3: T2-weighted image of rat brain 30 minutes after the third mannitol infusion. **A**: Treated brain. Note hyperintensity in right hemispheric cortical and deep gray regions, white matter structures, with associated swelling and midline shift. **B**: Untreated control rat brain
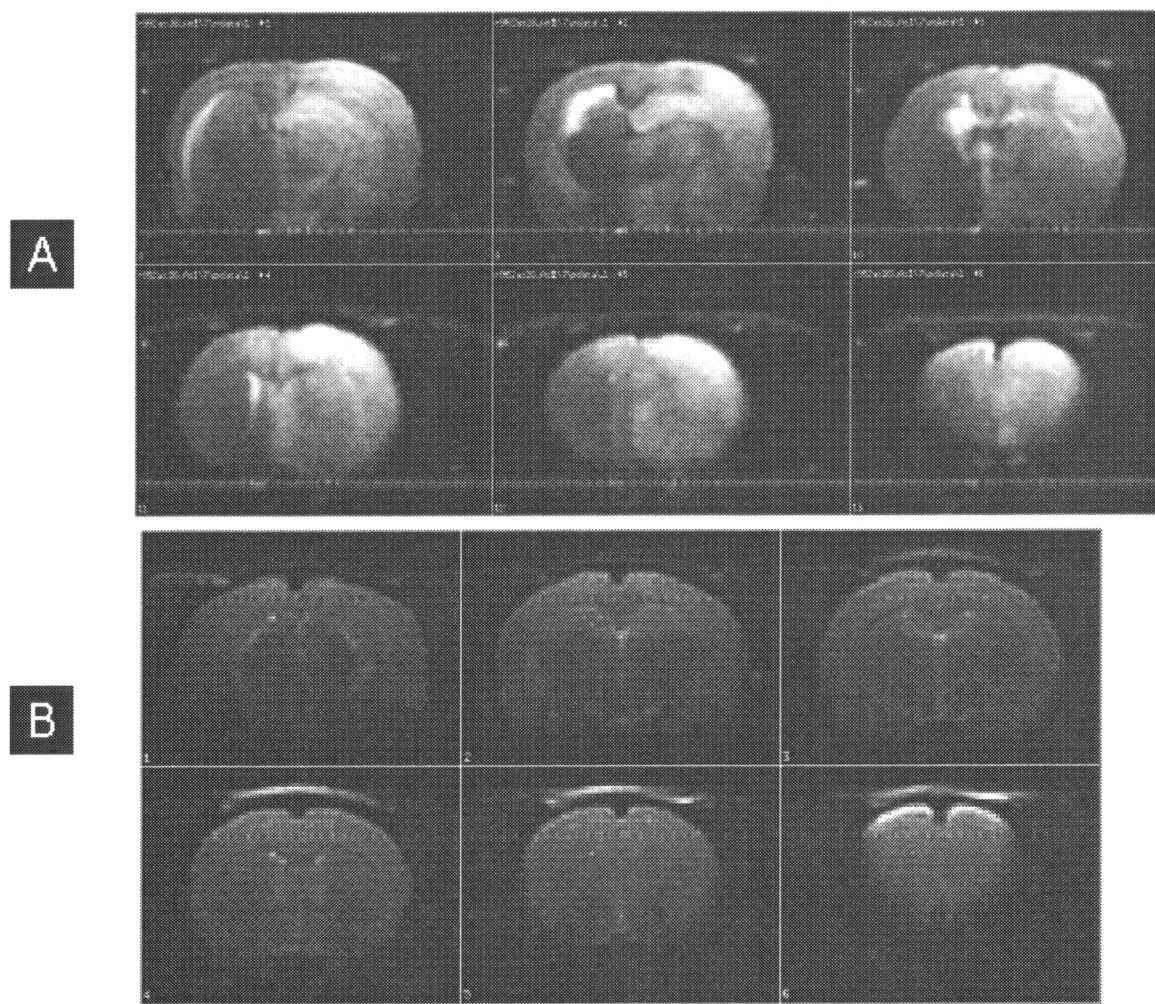
Figure 6-4: T2-weighted image of rat brain 1 hour after the third mannitol infusion. **A**: Treated brain. Note hyperintensity in right hemispheric cortical and deep gray regions, white matter structures, with associated swelling and midline shift. **B**: Untreated control rat brain.
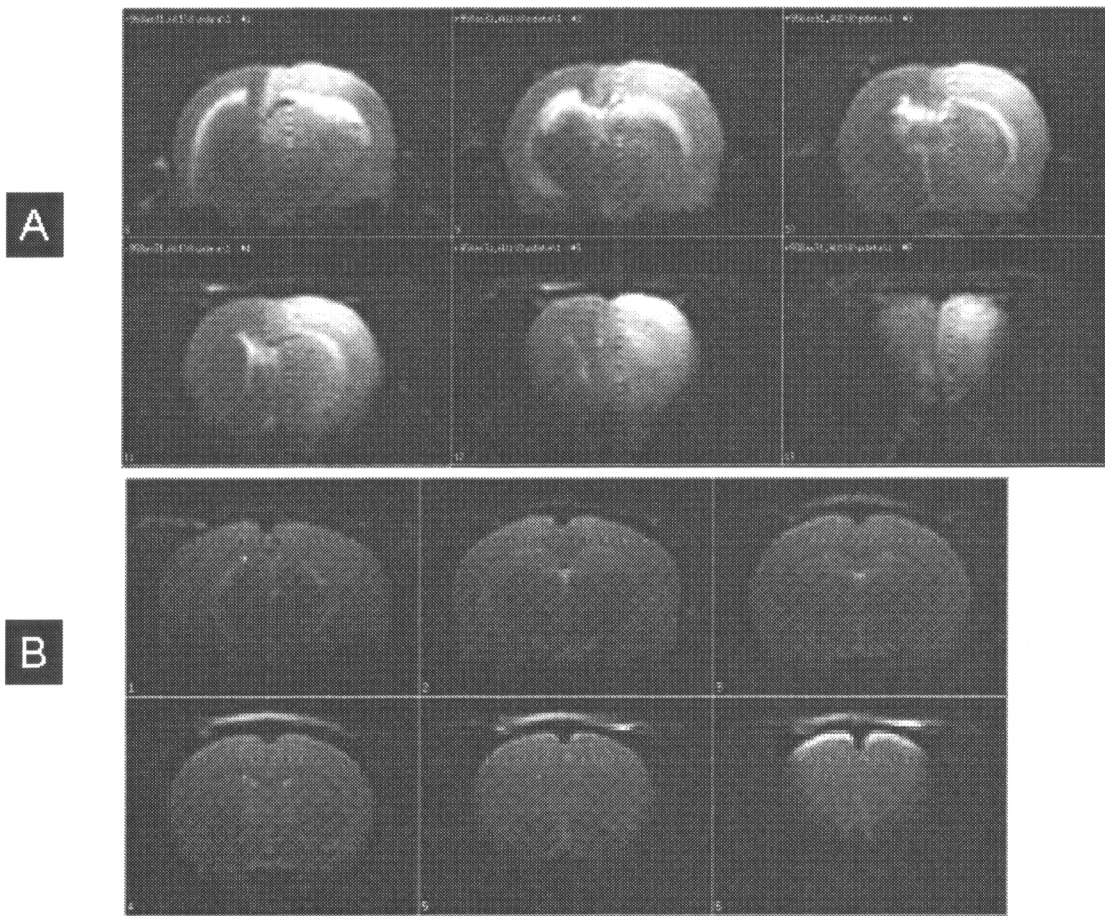
Figure 6-5: T2-weighted image of rat brain 24 hours after the third mannitol infusion.
A: Treated brain. Note localized hyperintensity in right cortical gray regions and
underlying white matter. **B**: Untreated control rat brain
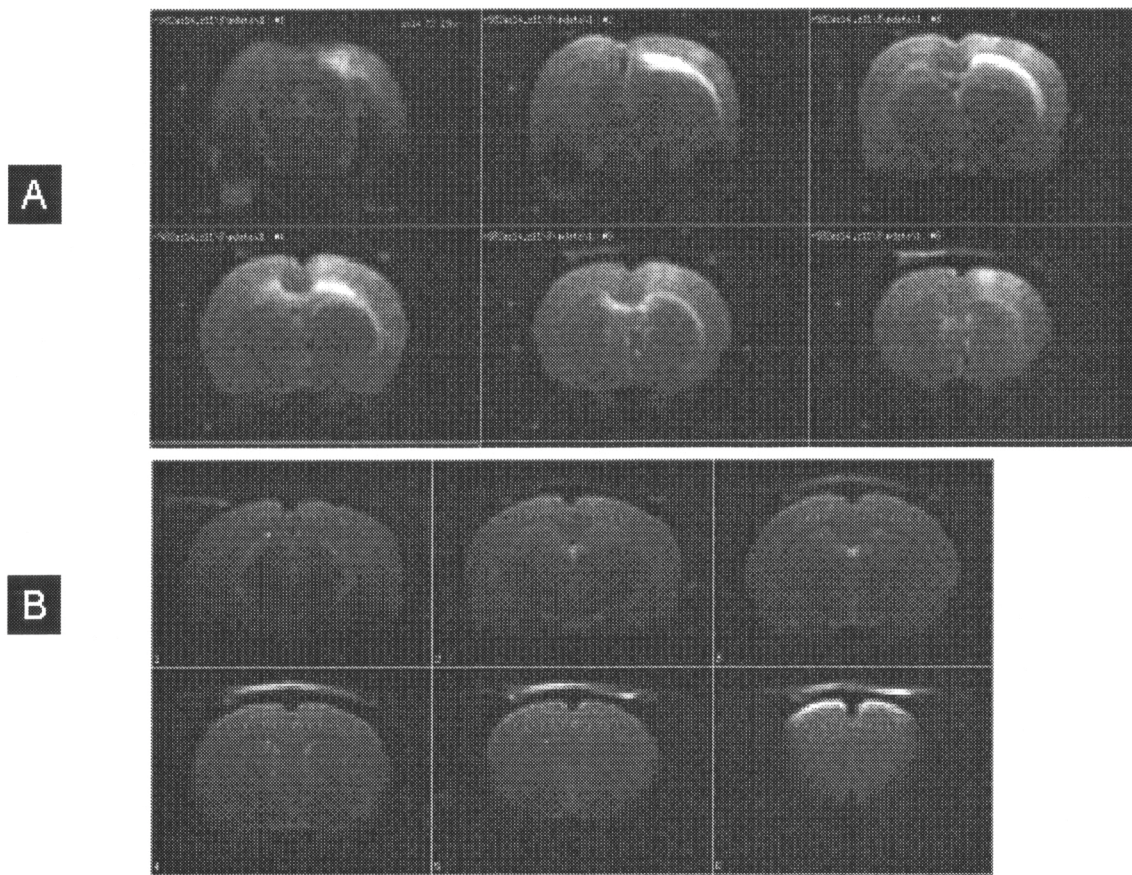
Figure 6-6: T2-weighted image of rat brain 48 hours after the third mannitol infusion. **A**: Treated brain. Note overall intensity in right hemispheric gray matter matches intensity of contralateral hemisphere. Some remnant hyperintensity in right cortical gray regions and white matter exist. **B**: Untreated control rat brain
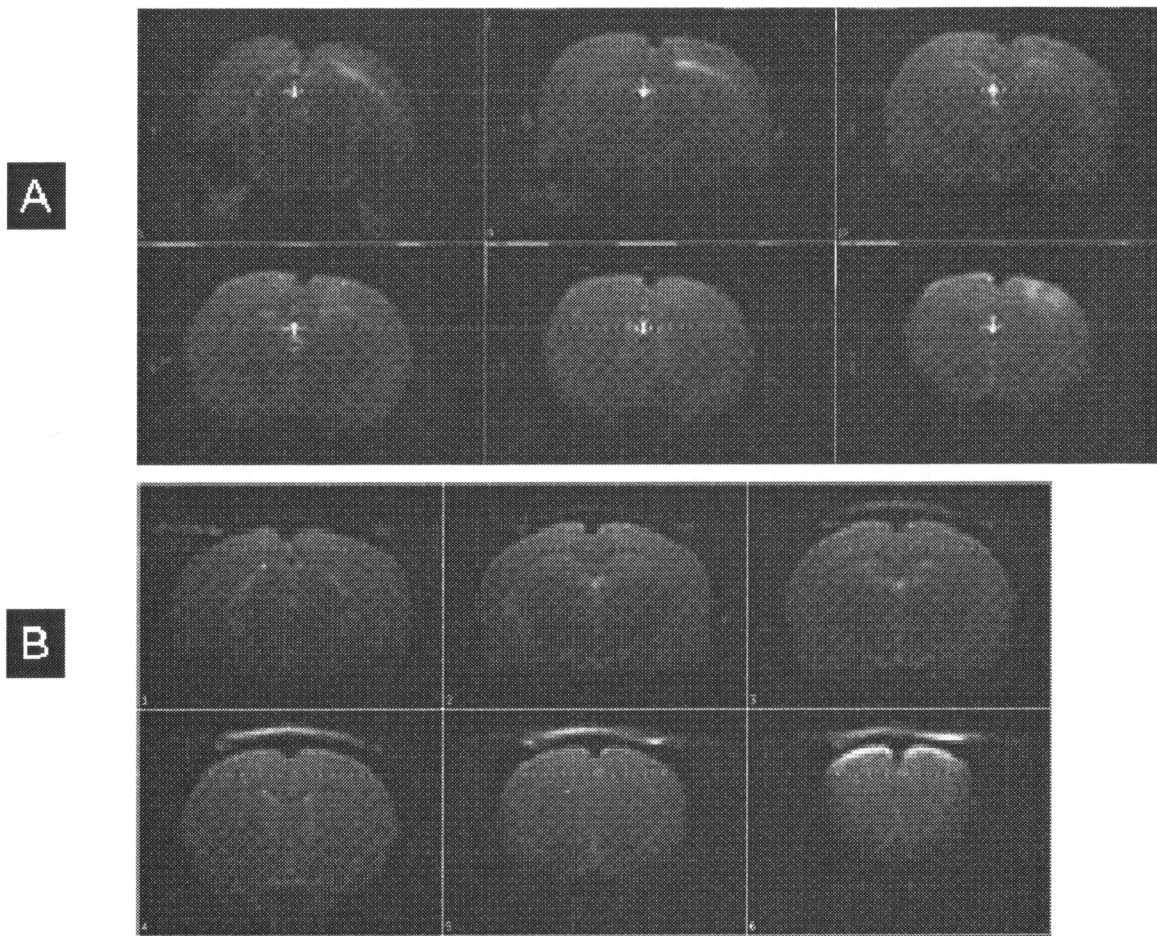
Water Maps

Water maps obtained 30 minutes and 1 hour after mannitol infusion displayed hyperintensity in the right cortical and deep gray regions, ipsilateral to mannitol perfusion. As shown in **Figure 6-7**, these regions appear to be analogous to hyperintensity observed in correlate T2W images obtained from the same animal 1 hour post infusion. Water maps obtained at later time points did not show evidence of intensity difference between the hemispheres.

Water maps provided water fraction (f_w) values that were extracted via region of interest (ROI) analysis described in the previous chapter. **Figure 6-8** contains graphs that show changes of f_w values over time after mannitol infusion, for cortical, deep and average gray matter. Values at 0 hours represent control f_w values in untreated brains. Average gray matter had a normal f_w of 77.8% in the right hemisphere and 77.9% in the left (**Figure 6-8 A**). Within 30 minutes of mannitol infusion, averaged ipsilateral gray matter (right hemisphere) displayed a water fraction of 83.8% versus a level of 78.3% seen in the contralateral gray matter (left hemisphere). There was a statistically significant difference observed between the hemispheres ($p<0.05$) which remained high after 1 hour, where f_w was increased to 84.8% in the right hemisphere compared to 78.3% in the left, as indicated by the asterisks on the graph. The f_w values dropped to near normal values at 24 and 48 hours, with no significant difference existing between right and left hemispheres.

A similar trend was observed when the cortical and deep gray regions were analyzed separately. Cortical gray tissue had a normal f_w of 79.3% and 79.2% in the left and right hemispheres, respectively (**Figure 6-8 B**). At both 30 minutes and 1 hour, the

right gray matter showed a higher average than the left, which was statistically significant (p<0.05). The right cortical gray matter showed a rise in f_w to 85.5% after 30 minutes and 86.3% after 1 hour. The contralateral left cortical gray matter remained at normal levels after 30 minutes, however, increased to 81.0% after 1 hour. The left cortical gray average at 1 hour produced a p-value of 0.048 using a t-test compared with the normal values (at time 0), which suggests a statistical difference (p<0.05). The left hemisphere also showed a difference in f_w at 48 hours that was higher and statistically different from normal (p=0.025). Right hemispheric cortical gray f_w values dropped after 24 and 48 hours. Right and left cortical gray f_w values were not significantly different between each other after 24 and 48 hours; however, the right cortical gray had an elevated f_w at 24 hours (80.9%) that was statistically significant when compared to the normal right cortical value (79.2%). Deep gray (caudate/putamen) tissue had a normal f_w of 76.3% for the left and 76.7% for the right hemisphere, which appeared to be less than the normal f_w observed in cortical regions (**Figure 6-8 C**). The right deep gray matter showed higher f_w values after 30 minutes (82.0%) and 1 hour (83.2%) when compared to the left deep gray matter that remained near 77%, that were statistically different (p<0.05). The right hemisphere dropped to near normal at 24 (77.9%) and 48 hours (77.9%) with no statistically significant difference from the left hemisphere. The left hemisphere remained near normal through the 24 and 48 hour observations with no statistically significant change from normal values as seen in the cortical gray. Sham-operated rats displayed normal water values at 2 hours and 48 hours post-surgery, with no statistically significant difference in the values between the hemispheres and when compared to normal brain tissue.

Figure 6-7: Water Map image of rat brain 1 hour after the third mannitol infusion. **A**: Treated brain. Note hyperintense regions in right hemisphere. **B**: T2 images of corresponding slices from same treated brain.
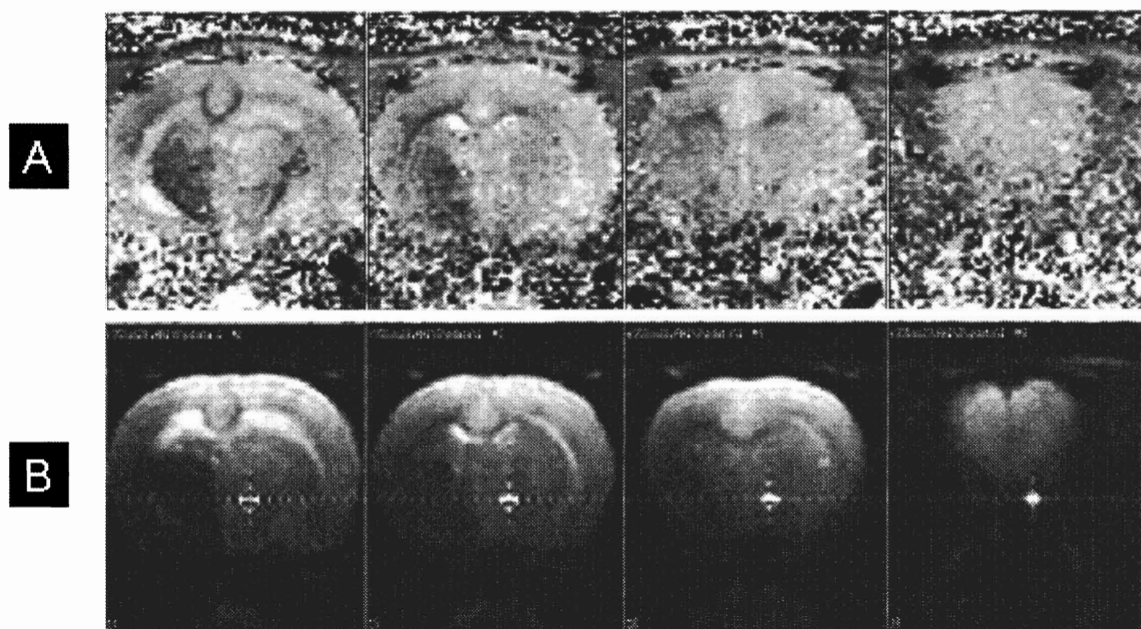
Figure 6-8: Graph of water fraction (f_w) changes in gray matter after mannitol delivery. **A**: Combined cortical and deep gray matter averages over time. **B**: Cortical gray matter changes over time. **C**: Deep gray matter (caudate/putamen) changes over time.
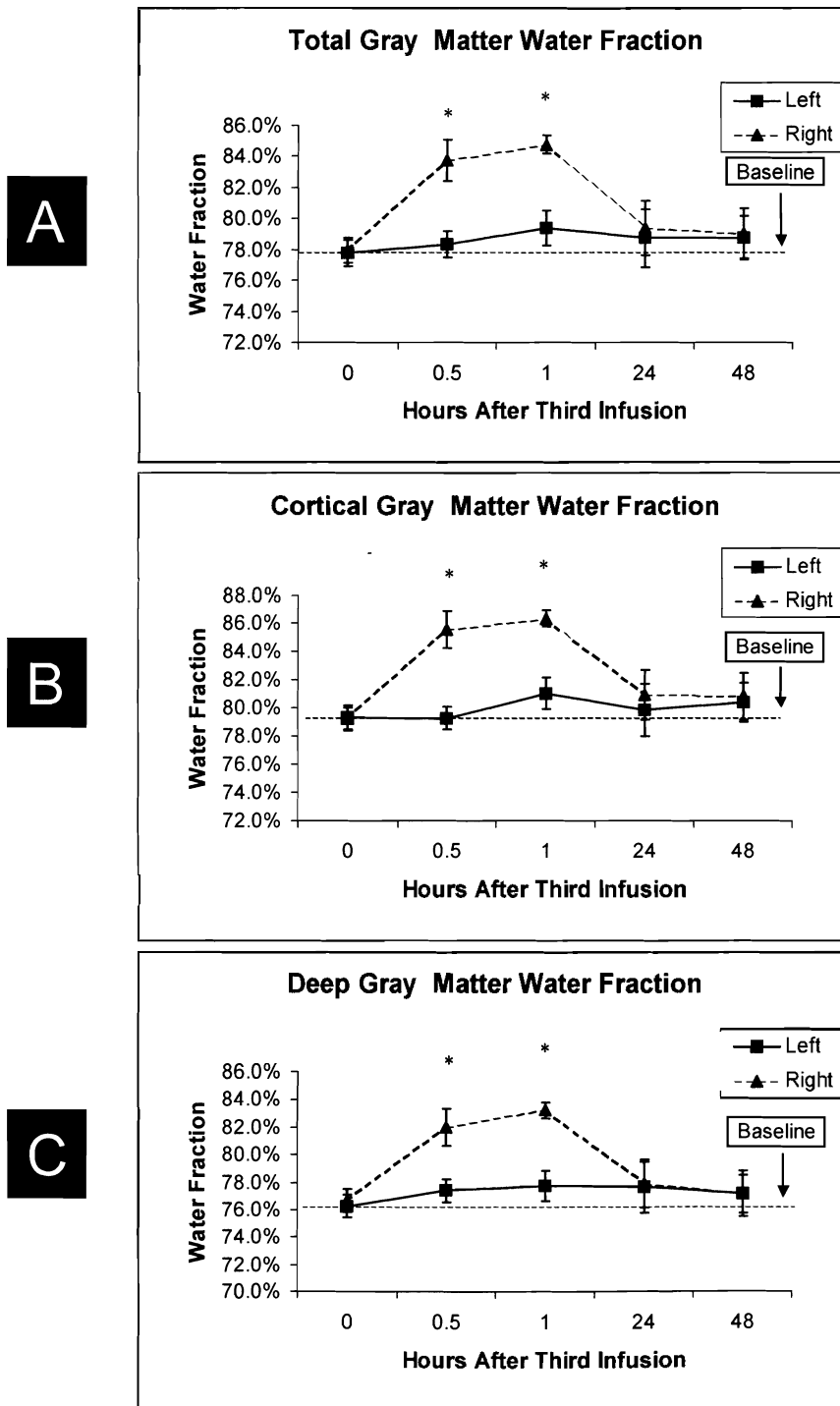
Apparent Diffusion Coefficient Maps

ADC maps obtained 30 minutes and 1 hour post mannitol infusion showed some

hyperintensity in the right hemispheric cortical and deep gray regions, when compared to

the contralateral hemisphere. There is also a hyperintensity observed in the white matter

tracts through the corpus callosum. **Figure 6-9** displays the ADC map obtained at the 1-

hour mark in the same animal whose water map is shown in **Figure 6-8**. This is a

representative ADC map, where hyperintense regions were not as pronounced as seen in

T2W images and water maps.

ADC ROI analysis was conducted in a manner similar to water map analysis.

Figure 6-10 contains three graphs corresponding to the average gray, cortical gray and

deep gray (caudate/putamen) ADC value changes over time. Values at 0 hour represent

control ADC values in untreated animals. Overall, the average gray matter had normal

ADC values of 0.58×10^{-3} mm^2/sec in left and right hemispheres (**Figure 6-10 A**). After

mannitol infusion, average gray values were 0.53×10^{-3} mm^2/sec in the left hemisphere

and 0.51×10^{-3} mm^2/sec in the right hemisphere, 30 minutes after infusion. After 1 hour,

these values were 0.45×10^{-3} mm^2/sec in the left hemisphere, while remaining at 0.51×10^{-3}

mm^2/sec in the right hemisphere. Of note, the differences between the hemispheres were

not statistically significant at these two time points. Also, there was no statistically

significant change in average gray matter values when compared to normal brain tissue

from the 0 time measurements or from untreated control animals. After 24 hours,

hemispheric average gray matter ADC was 0.54 mm^2/sec in the left hemisphere and $0.64 \times$

10^{-3} mm^2/sec in the right hemisphere. The right hemisphere gray matter had a higher ADC

Figure 6-9: ADC images of rat brain 1 hour after the third mannitol infusion. Note hyperintense regions in right hemisphere.

Figure 6-10. Graph of ADC changes in gray matter after mannitol delivery. **A**: Combined cortical and deep gray matter averages over time. **B**: Cortical gray matter changes over time. **C**: Deep gray matter (caudate/putamen) changes over time.
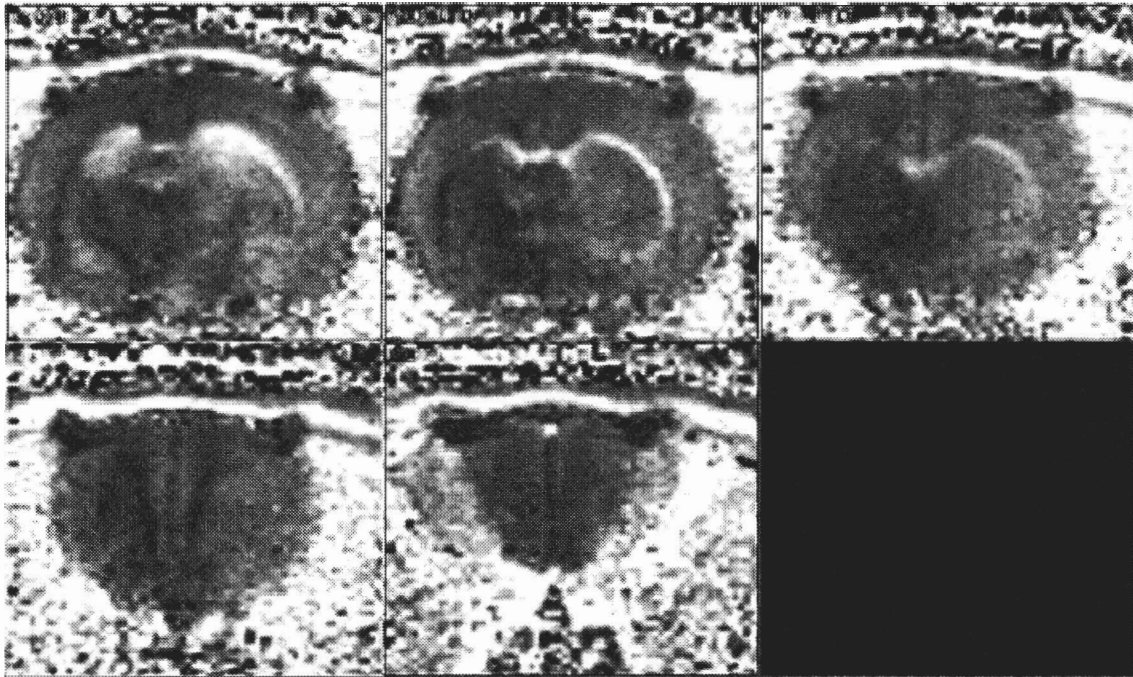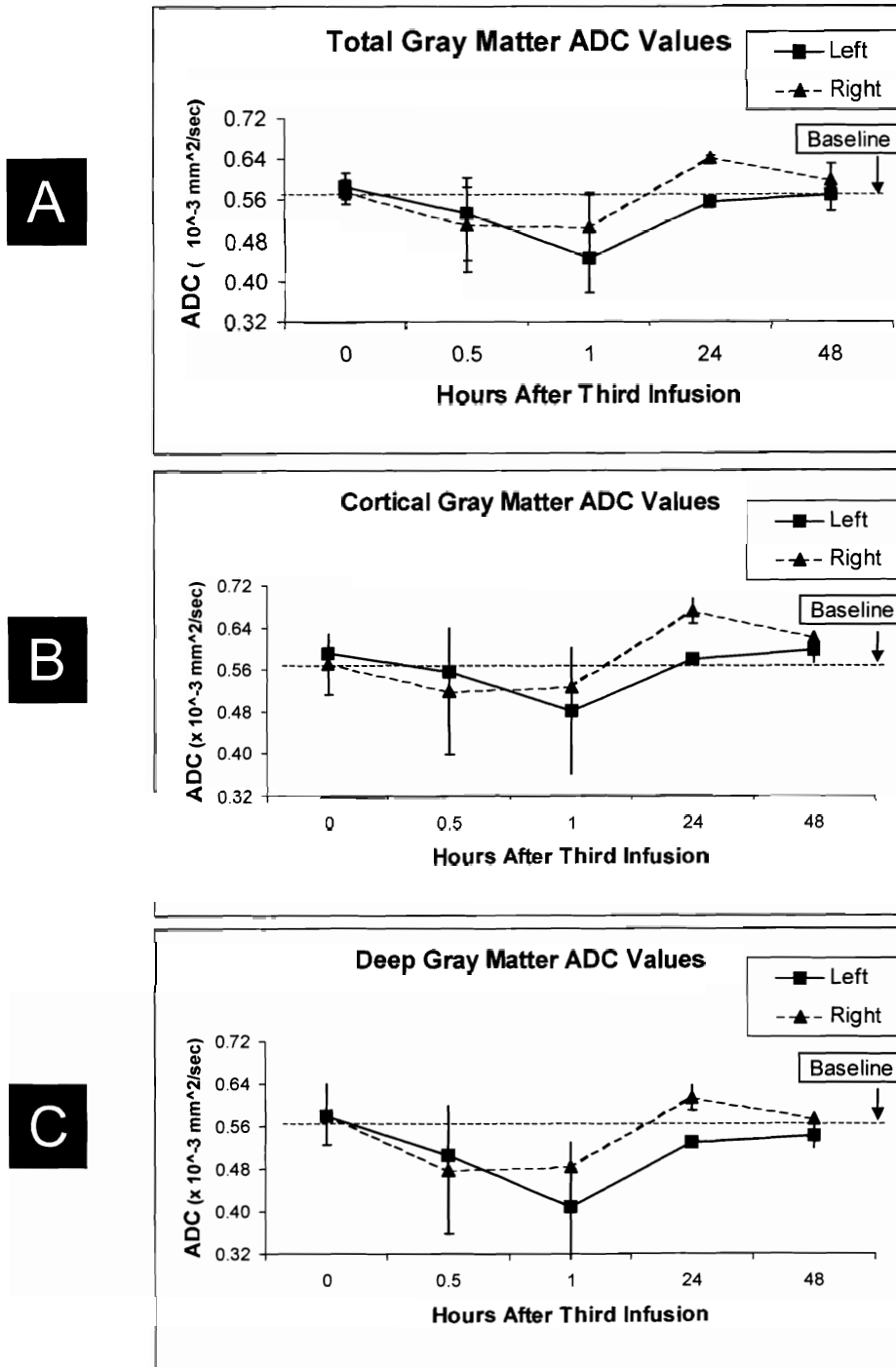
than the left after 24 hours, and this difference was statistically significant ($p<0.05$). When compared to normal tissue ADC from the 0 time measurements, each hemisphere also showed a statistically significant difference at the 24-hour mark. After 48 hours, the average gray matter ADC was near normal values with no statistically significant differences observed.

When observed separately, cortical gray matter is seen to follow the same pattern as the average gray matter values (**Figure 6-10 B**). The normal cortical gray matter ADC was measured to be 0.59×10^{-3} mm^2/sec in the left hemisphere and 0.57×10^{-3} mm^2/sec in the right hemisphere. The left and right cortical gray matter ADC values were 0.56×10^{-3} mm^2/sec and 0.52×10^{-3} mm^2/sec, respectively, 30 minutes after mannitol infusion. After 1 hour, the left cortical gray matter ADC value was 0.48×10^{-3} mm^2/sec, while the right cortical gray matter value was 0.53×10^{-3} mm^2/sec. The differences between the left and right cortical gray at 30 minutes and 1 hour were not statistically significant; nor were they individually statistically significant in difference from normal values. After 24 hours, the left cortical ADC value was 0.58×10^{-3} mm^2/sec, while the right cortical ADC was higher than normal at 0.67×10^{-3} mm^2/sec. The right cortical gray matter had a higher ADC from both the normal tissue and contralateral regions that was statistically significant ($p<0.05$). After 48 hours the ADC values were near normal with no statistically significant differences.

The deep gray ADC values followed the same pattern of change observed in the cortical and overall gray matter, with some differences (**Figure 6-10 C**). The normal ADC values in the deep gray were observed to be 0.58×10^{-3} mm^2/sec in the left and right deep

gray matter. 30 minutes after mannitol infusion, the ADC values were 0.51 x 10^{-3} mm^2/sec

and 0.48 x 10^{-3} mm^2/sec in the left and right deep gray matter, respectively. The average

ADC in the left deep gray matter was 0.41 x 10^{-3} mm^2/sec after 1 hour, while the right

deep gray average ADC value remained at 0.48 x 10^{-3} **mm^2/sec.** There was no statistically

significant difference found between the hemispheres at these time points or when

compared to normal tissue. After 24 hours, the deep gray matter ADC values were 0.53 x

10^{-3} mm^2/sec in the left hemisphere and 0.61 mm^2/sec in the right hemisphere. At 24

hours, the difference observed between left and right deep gray ADC was statistically

significant (p<0.05). In addition, both right and left deep gray matter ADC values were

statistically significant in difference when compared to normal ADC values. The ADC

values in the left deep gray matter was 0.54 x 10^{-3} mm^2/sec after 48 hours. This difference

from normal values was statistically significant. After 48 hours, the right deep gray ADC

returned to the normal value of 0.58 x 10^{-3} mm^2/sec. Sham-operated rats displayed normal

ADC at 2 hours and 48 hours post surgery, with no statistically significant differences.

Light Microscopy

Brain tissue extracted from cortical and deep gray regions in control, sham-

operated, and 2 hours post mannitol infusion were observed using light microscopy (LM)

under hematoxylin and eosin (H&E) staining. Cortical gray regions in the left hemisphere

contralateral to infusion (**Figure 6-11**) appeared to contain healthy neurons and normal

blood vessels when compared to analogous regions in untreated control animals (**Figure 6-

14**). In the infused brains, the right hemisphere showed marked differences in structures

when compared to the contralateral left hemisphere. As seen in **Figure 6-11 B1 and B2**, the right cortical gray regions contained perivascular spaces surrounding the overwhelming majority of blood vessels. Also present were perineuronal spaces surrounding the majority of neurons. The neurons themselves appeared to be shrunken and dark in the ipsilateral perfused cortical gray matter when compared to the neurons in the contralateral hemisphere (**Figure 6-11 A1 and A2**). Also observed was a spongy appearance in the neuropil in the right cortical gray matter, which appeared more uniform and dense in the contralateral left cortical gray region.

In **Figure 6-12**, similar results are shown for the deep gray matter (caudate/putamen) of the mannitol-infused rat brain. These images are from the same rat brain as seen in **Figure 6-11.** As noted earlier, the left hemisphere contralateral to mannitol infusion (**Figure 6-12 A1 and A2**) appears to contain blood vessels and neurons that are comparable to those seen in the control deep gray regions. We also see a similar perivascular white space surrounding virtually all blood vessels in the deep gray region of the right hemisphere (**Figure 6-12 B1 and B2**). The perineuronal space surrounding dark, shrunken neurons were not as prevalent in the ipsilateral right deep gray region when compared to the same hemisphere's cortical gray matter. The distributed bundled tracts that appear throughout the caudate region are seen as disparate pale regions in the neuropil. These bundles appear uniform in the contralateral deep gray matter, but take on an irregular appearance in the ipsilateral right caudate region.

Figure 6-11. Histological sections of cortical gray matter (H&E stain), 2 hours after last mannitol infusion. **A1**: Left cortical gray matter, in hemisphere contralateral to mannitol perfusion (x40). **A2**: Enlarged region (white rectangle in A1) in left cortical gray matter showing blood vessel (asterisks) and neuron (black arrow) (x100). **B1**: Right cortical gray matter, in hemisphere ipsilateral to mannitol perfusion (x40). **B2**: Enlarged region (white rectangle in B1) in right cortical gray matter with dark, shrunken neuron with perineuronal space (black arrow) and blood vessels with perivascular space (asterisks) (x100).
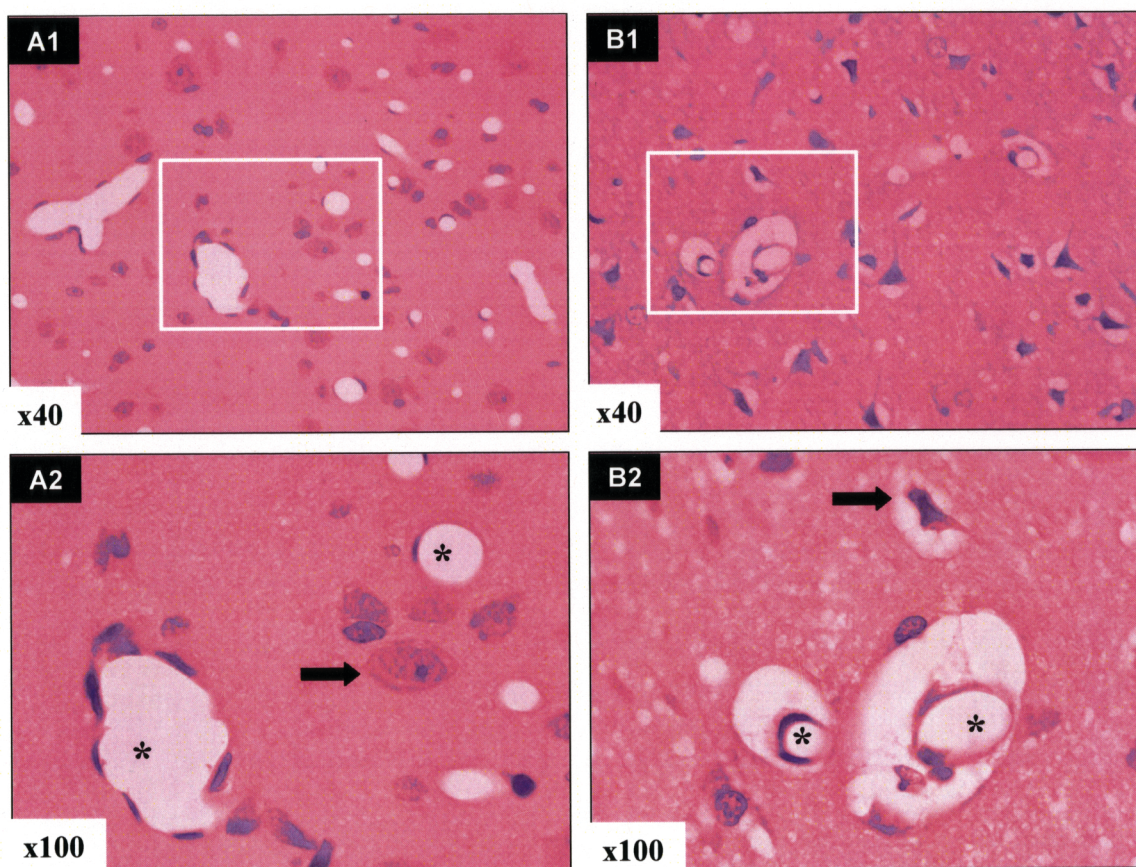
Figure 6-12. Histological sections of deep gray matter (caudate/putamen), 2 hours after last mannitol infusion. **A1**: Left deep gray matter, in hemisphere contralateral to mannitol perfusion (x40). **A2**: Enlarged region (white rectangle in A1) in left deep gray matter showing blood vessel (asterisks) and neuron (black arrow) and tract bundles (white arrows) (x100). **B1**: Right deep gray matter, in hemisphere ipsilateral to mannitol perfusion (x40). **B2**: Enlarged region (white rectangle in B1) in right deep gray matter with dark, shrunken neuron with perineuronal space (black arrow) and blood vessels with perivascular space (asterisks), also note lack of distributed bundles seen in A2 (x100).
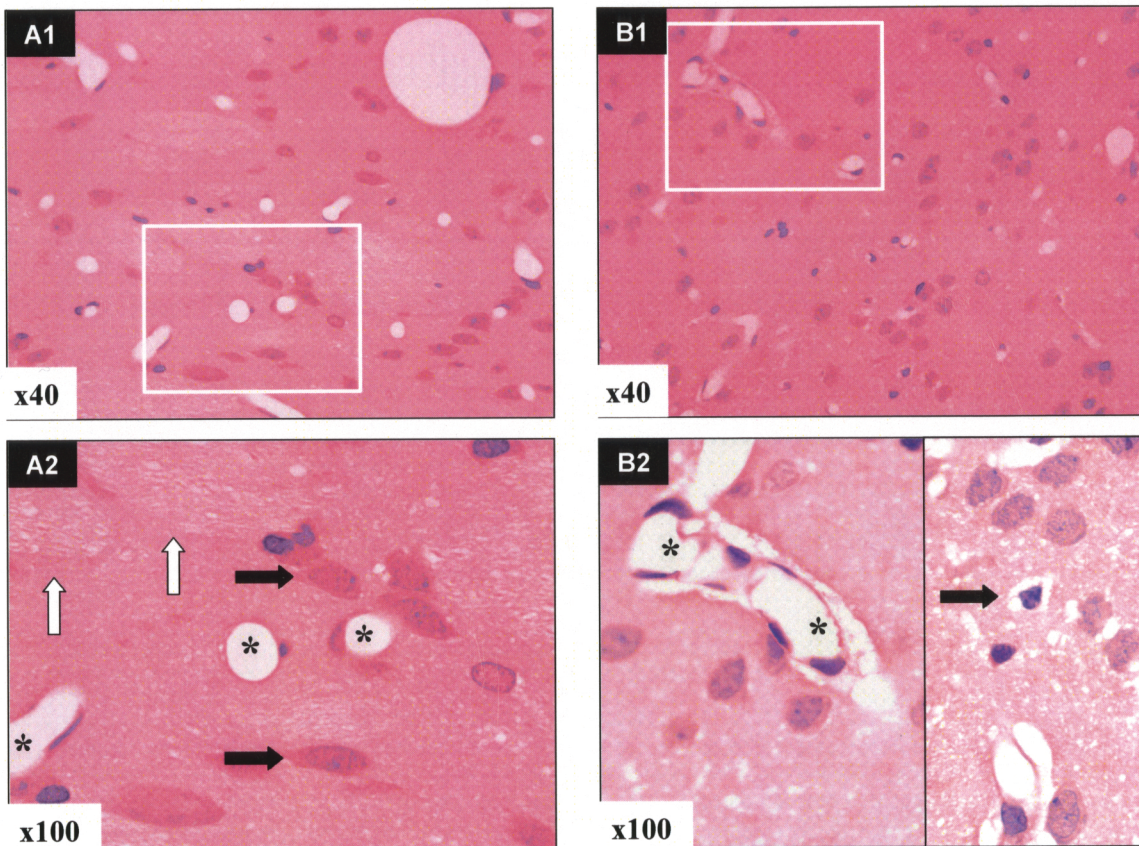
Figure 6-13. Histological sections of cortical gray and deep gray (caudate/putamen) (H&E stain), 2 hours after sham surgery. **A1**: Right cortical gray matter, in hemisphere ipsilateral to ligated CCA (x40). **A2**: Enlarged (white rectangle from A1) area of right cortical gray matter with blood vessel (asterisks) and neuron (black arrow) indicated (x100). **B1**: Right deep gray (caudate/putamen) matter in hemisphere ipsilateral hemisphere to ligated CCA (x40). **B2**: Enlarged (white rectangle from B1) area of right deep gray matter with neuron (black arrow), blood vessel (asterisks) and tract bundle (white arrow) indicated (x100).
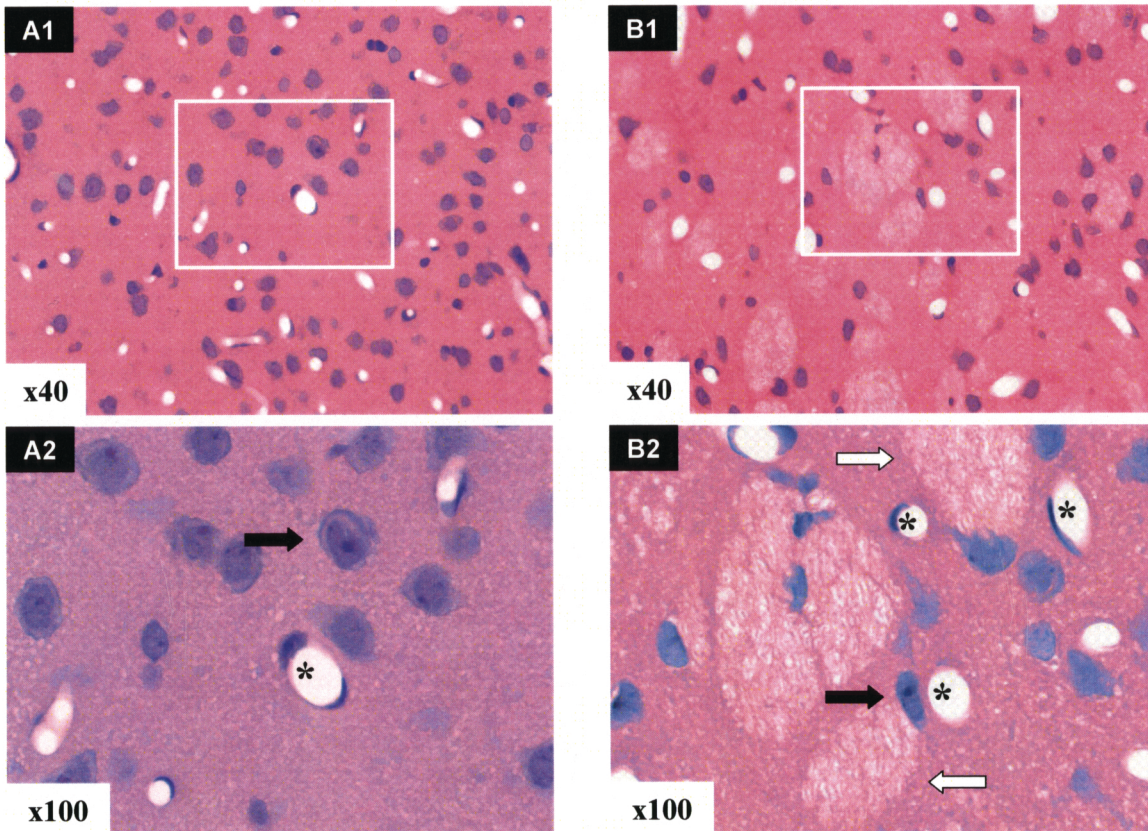
Figure 6-14. Histological sections of cortical gray and deep gray (caudate/putamen) (H&E stain) from untreated control animals. **A1**: Right cortical gray matter (x40). **A2**: Enlarged (white rectangle from A1) area of right cortical gray matter with blood vessel (asterisks) and neuron (black arrow) indicated (x100). **B1**: Right deep gray matter (x40). **B2**: Enlarged (white rectangle from B1) area of right deep gray matter with neuron (black arrow), blood vessel (asterisks) and tract bundle (white arrow) indicated (x100).
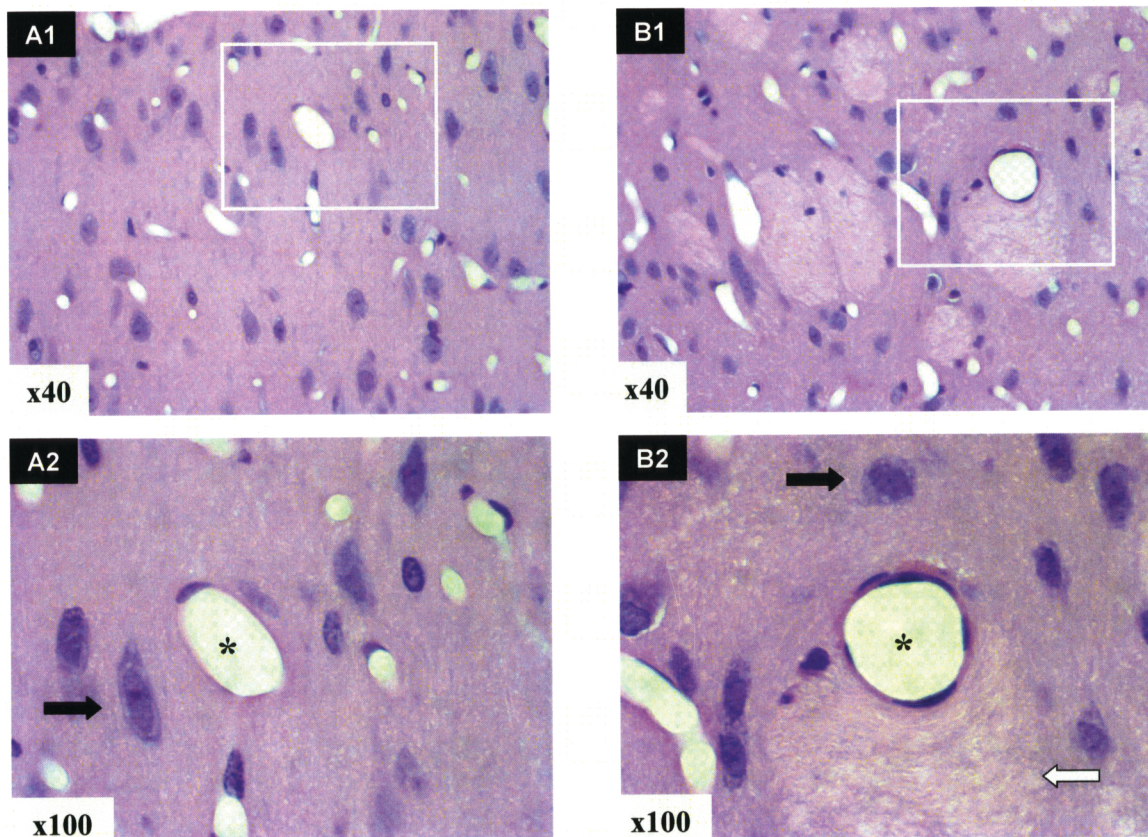
Representative images of the cortical and deep gray regions in sham-operated rats are shown in **Figure 6-13**. The blood vessels, neurons and overall neuropil appear identical to the analogous regions in the untreated control brain shown in **Figure 6-14**.

Transmission Electron Microscopy

Transmission electron microscopy (TEM) was performed on the right cortical gray regions of normal rats and in cortical gray regions ipsilateral and contralateral to mannitol infusion. **Figure 6-15** depicts representative images of blood vessels and neurons in an untreated animal and an animal sacrificed 2 hours after the third mannitol infusion (this example is from the same rat shown in LM photographs discussed above). The contralateral cortical gray structures (**Figure 6-15 B and E**) appear similar in morphology to those found in the control cortical gray matter (**Figure 6-15 C and F**).

As seen under LM, there is a marked difference in morphology of the region surrounding blood vessels and neurons in the mannitol perfused cortical gray when compared to similar regions in the contralateral and control tissue. In perfused tissue, perineuronal space observed in LM pictures appears to be swollen processes surrounding the neuron as seen in **Figure 6-15 A**. These white areas appear to be membrane-enclosed fluid spaces with free-floating mitochondria. The neuron in **Figure 6-15 A** also appears to have a scalloped shaped due to the surrounding swollen processes. In addition, when compared to the contralateral and normal neurons, the neuron located in the right cortical gray appears to have a denser cytoplasm. The mitochondria inside the cytoplasm appear similar to those in the normal and contralateral neurons. The capillary shown in **Figure 6-**

15 D exhibits the perivascular space observed in LM images earlier. Upon closer

examination, this space may be due to swollen astrocytic processes surrounding the blood

vessel as evidenced by membrane and mitochondria free floating in the watery spaces.

The neuropil surrounding the neuron and blood vessel in the perfused tissue

appears to be more irregular in distribution when compared to contralateral and normal

tissue. There seem to be a great deal of white spaces in this tissue that can be mostly

attributed to swollen cellular processes. **Figure 6-16** contains images of neuropil

surrounding blood vessels in the mannitol-perfused and normal tissue, shown previously in

Figures 6-15 D and F, respectively. Upon closer examination of the neuropil in the

perfused hemisphere (**Figure 6-16 A2**) there are white areas which seem to be enclosed by

cellular process, however, some irregular white regions appear to be fluid-filled space

which may be ECS. This putative ECS seems to be undistinguishable in the denser

neuropil of normal tissue (**Figure 6-16 B**), which appears quite packed and dense in

appearance.

Gd-DTPA Infusion

Figure 6-17 depicts a T1-map representative of gadolinium-diethylene-triamine penta-

acetic acid (Gd-DTPA) infusion. This image shows a series quantitative T1 map images

acquired every 10 minutes during the course of a 50 minute Gd-DTPA infusion and 80

minute follow-up, 130 minutes total. Time 0 shows the normal frontal cortical gray region,

after which infusion begins as indicated. The Gd-DTPA appears as a dark region in the

right cortical gray due to the low relaxivity attributed to Gd. The Gd-DTPA appears

Page Missing

Figure 6-15. TEM images from right hemispheric cortical gray region in mannitol infused, sham-operated and control rats. **A**: Neuron in cortical gray matter of rat, 2 hours post mannitol infusion (x2500). **B**: Neuron in cortical gray matter of sham-operated rat, 2 hours post-surgery (x2500). **C**: Neuron in cortical gray matter of untreated control rat (x2500). **D**: Blood vessel in cortical gray matter of rat, 2 hours post mannitol infusion (x2500). **E**: Blood vessel in cortical gray matter of sham-operated rat, 2 hours post-surgery (x2500). **F**: Blood vessel in cortical gray matter of untreated control rat (x2500).
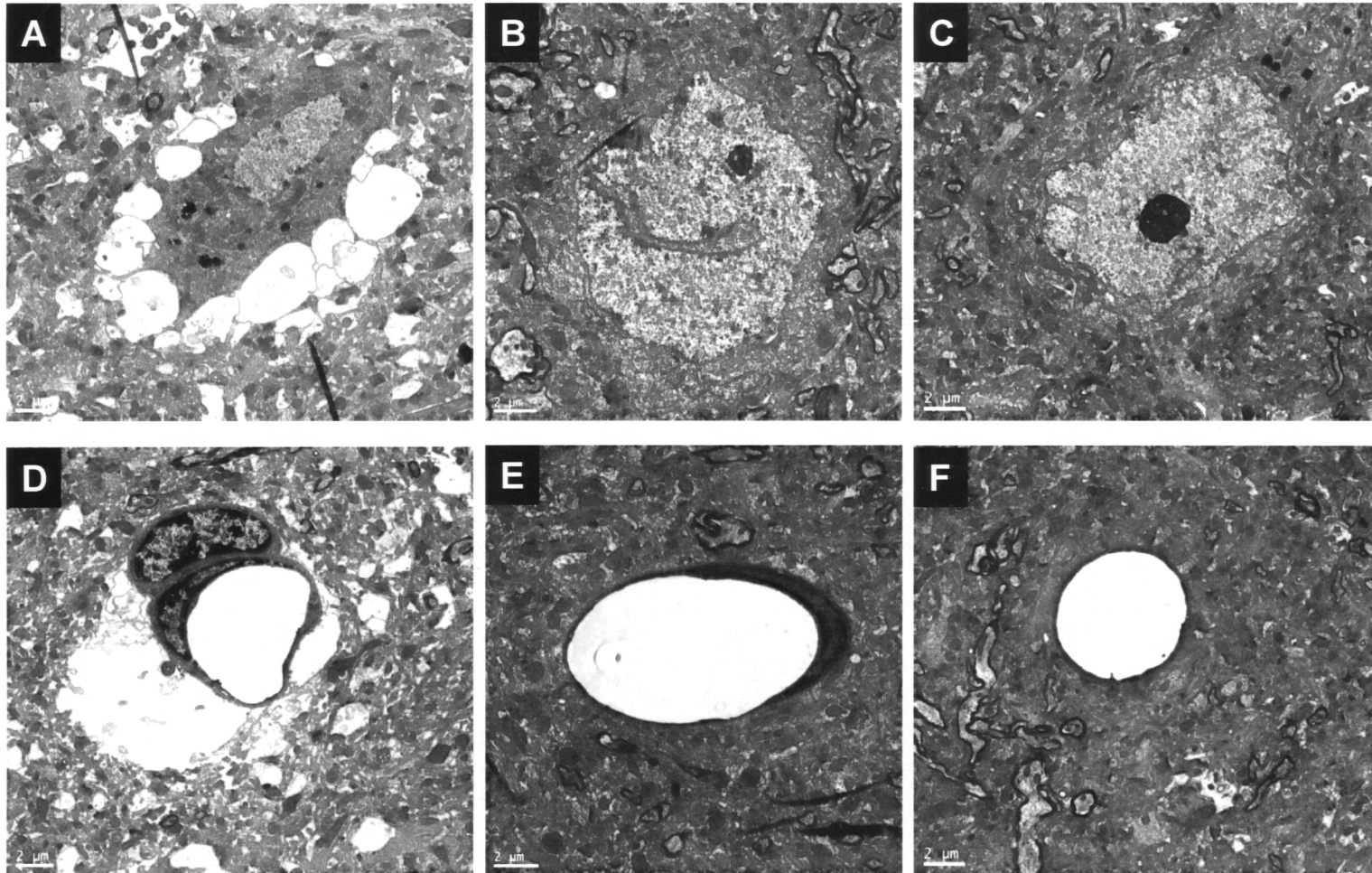
Figure 6-16. TEM images of neuropil near blood vessels in right cortical gray regions of mannitol infused and untreated control brains. **A1:** Neuropil surrounding blood vessel in right cortical gray matter ipsilateral to mannitol infusion (x2500). **A2:** Neuropil region enlarged from white box in A1 (x10,000). **B1:** Neuropil surrounding blood vessel in right cortical gray matter of untreated control rat (x2500). **B2:** Neuropil region enlarged from white box in B1 (x10,000).
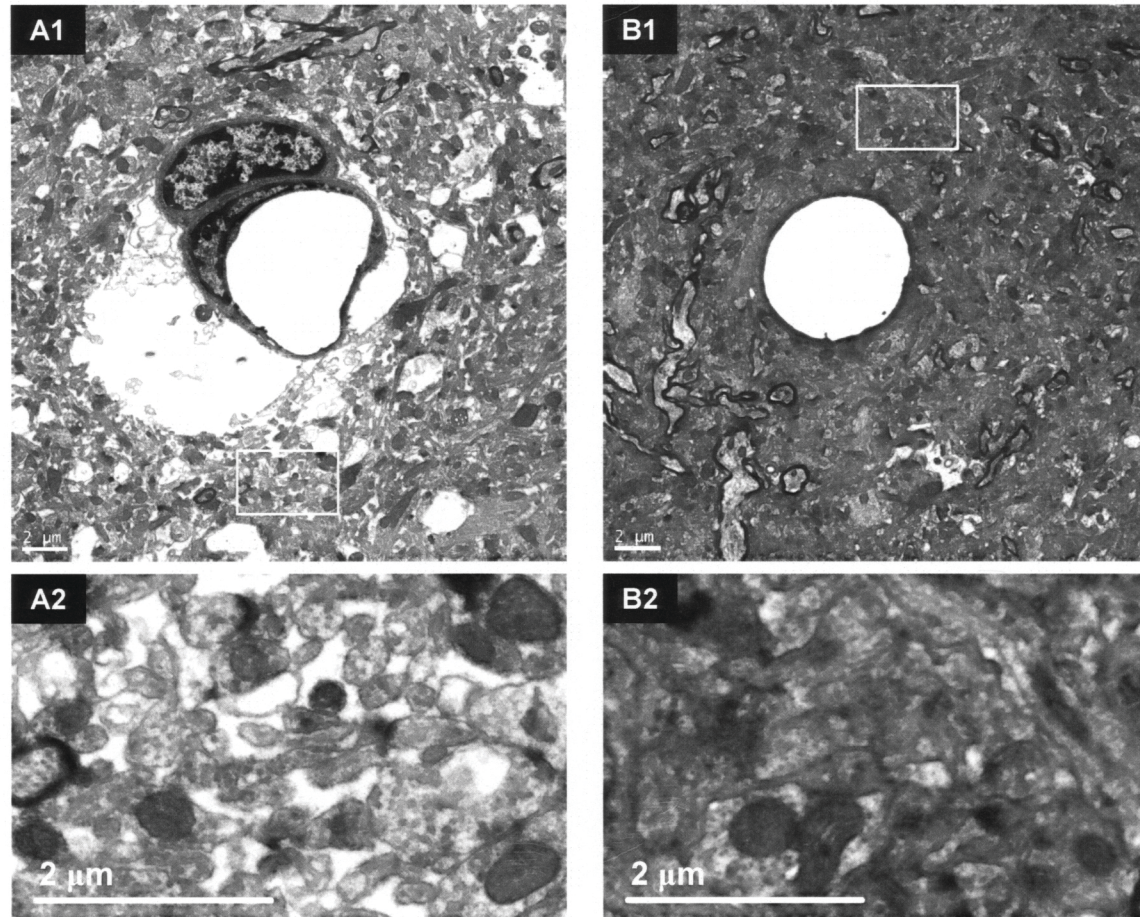
to be isolated to the right cortical region throughout the infusion, and once infusion ends at

the 50-minute mark, the Gd-DTPA appears to dissipate based on the observed return to

baseline contrast.

Figure 6-17. Time series T1 Map of Gd-DTPA infusion in frontal cortical gray matter of a normal brain. Infusion begins at time 0 and ends after 50 minutes, as indicated on the diagram. Note infused Gd-DTPA appears as a dark region in right hemisphere due to the decrease in T1 value caused by the Gd relaxivity effect.
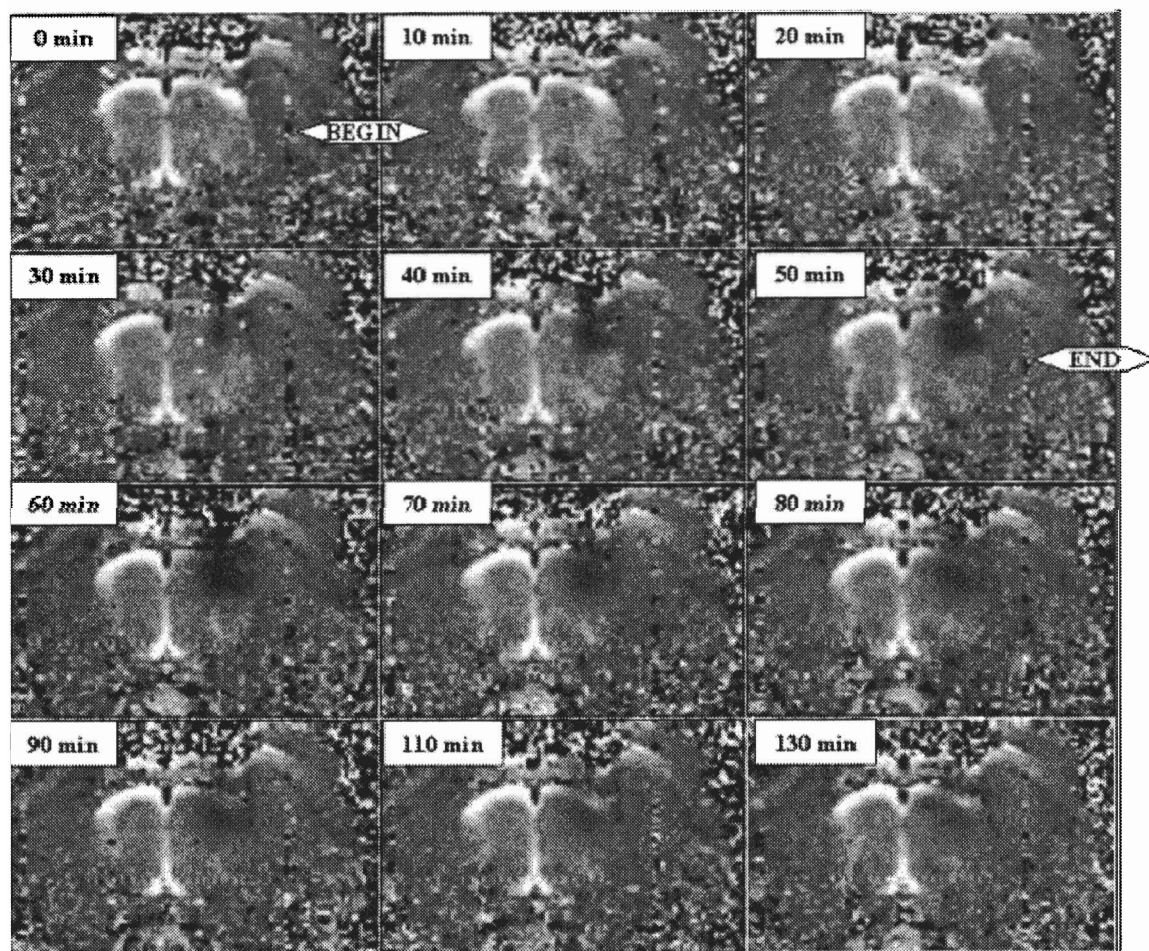
CHAPTER 7

DISCUSSION

Understanding the dynamics of CED under pathological brain states is vital for proper drug targeting and dosage. Previous studies by Haar characterized this convective delivery in CE.[3] However, CED under VE proved inconclusive due to limitations attributed to the direct infusion VE model.[3] Therefore, the current study looked to find a better model to study CED in VE conditions.

The mannitol infusion model of VE was selected to be characterized and evaluated for CED study. The mannitol model was modified from two infusions of 25% mannitol[55] to three infusions, based on preliminary studies we conducted in rat brain, using T2W imaging as an initial criterion for edema formation. The preliminary studies indicated a widespread edema formation through the cortical and deep gray matter, based on hyperintensity observed in T2W images. Consistent BBB disruption marked by EB dye suggested that this edema was VE in nature. Further MRI studies and histological results confirmed a unilateral widespread edema formation in gray matter ipsilateral to mannitol perfusion. Details on the characterization of this edema and specific implications for future study are discussed below.

Controls

The sham-operated animals did not demonstrate changes in ADC values when compared to normal untreated brain. Upon hematoxylin and eosin (H&E) staining, neurons and blood vessels appeared healthy in the gray matter ipsilateral to the common carotid artery (CCA) ligation. This was expected as previous studies have shown no acute ischemic effect from sacrificing the right CCA in a rat.[144] Our light microscopy (LM) results also suggested no ischemic injury from CCA ligation. Therefore, changes observed in the right hemisphere ipsilateral to mannitol infusion were due to the mannitol infusion specifically.

Collateral Effects of Mannitol Infusion

T2W imaging was utilized in preliminary experiments to gauge edema formation and led to the selection of the current mannitol model with three infusions. Mortality was high in our experiment, as 7 out of the 11 (64%) perfused animals appeared to lose spontaneous breathing 2 hours post mannitol infusion. This by itself would imply a high degree of toxicity associated with the mannitol infusions. With the marked water levels seen with this model, it may be that our initial use of T2 changes for titrating mannitol doses to obtain edema development may not provide conditions favorable for animal survival.

Edema formation

The T2W hyperintensity consistently observed in the cortical and deep gray matter was indicative of edema formation in the right hemisphere of the brain, ipsilateral to mannitol perfusion. This initial edema formation was seen as soon as 30 minutes after the series of mannitol infusions, and is even evident in cortical gray tissue after 24 hours. Water maps confirmed the presence of edema with significantly higher water values observed in the right hemisphere when compared to the left hemisphere, 30 minutes and 1 hour after mannitol delivery. Normal human gray and white matter was found to contain 69% and 80% f_w, respectively.[145] The current study found gray matter in the rat to have a normal average f_w of 78%. At 1 hour, water values in edematous deep and cortical gray matter demonstrated a 6% to 7% increase in water content compared to the contralateral gray matter. Although the increase in water content in the rat brain was extensive, larger increases have been observed in other animals and humans. Animals studies by Fatouros *et al.* have observed an increase of water content from the normal 68% seen in the white matter of cat brain to 78.6% in edematous white matter using the infusion model of VE.[146] The magnitude of edema increase in cat white matter was larger than what we observed in rat gray matter. Given that edematous fluid in the ECS preferentially flows in white matter,[147] this would be expected. Another study Fatouros and Marmarou found the f_w for an ROI centered on a human brain tumor to be as high as 86.7% versus 72.1% for the contralateral ROI.[148]

The water fraction (f_w) measured in the averaged gray and deep gray matter contralateral to perfusion remained near normal through all time periods. Therefore, the

observed gray matter edema was localized to the right hemisphere. When observed

separately, however, the cortical gray matter in the left hemisphere had statistically

significant high f_w observed after 1 hour and 48 hours when compared to normal cortical

gray water levels. There was a small rise in brain water in the left cortical gray matter,

despite the lack of cytotoxic injury or BBB disruption as verified by EB dye studies. In

conjunction with the bilateral hyperintensity observed in T2 images, these observations

would suggest the possibility of some contralateral flow of edema fluid from the right

cortical gray matter into the left cortical gray via white matter tracts, and would need to be

verified by future investigations. Overall, based on water map and T2 analysis, a large

cortical and deep gray region of edema was created within an hour of the series of mannitol

infusions and resolved within 48 hours.

Based on the series of processed T1 maps, the Gd-DTPA appeared to occupy a

volume of distribution that was enclosed in region of frontal cortex that consistently

showed T2 hyperintensity in other animals (**Figure 7-1 A and C**). As seen in **Figure 7-1

B and D,** Haar demonstrated Gd-DTPA distribution after CED in the caudate/putamen

region of normal rat brain that appears to occupy a similar region exhibiting consistent T2

hyperintensity in our edematous animals.[55] Gd-DTPA distribution results seen in the

frontal cortical gray and Haar's caudate region suggest the current model can be applied to

CED studies in both areas of the brain. Since this edema was prevalent within an hour of

infusion, and nearly gone after 24 hours, CED studies using the current model could be

conducted the same day as mannitol infusion. This model proved to be appropriate for

CED study in general edematous gray matter. However, further analysis of ADC and

histological results were then performed in order to determine whether the observed edema

demonstrated other important characteristics consistent with VE.

Characterizing the Edema

Mannitol delivery via the internal carotid artery (ICA) at the rate we used has been

shown to produce BBB disruption after just one bolus.[95] This is a reversible BBB opening

that closes within a period of 30 minutes.[21] We then reasoned that multiple mannitol

infusions spaced 30 minutes would create a prolonged opening of the BBB to allow flow

of proteinaceous fluid into surrounding parenchymal tissue, mimicking the pathological

state characteristic of VE. EB dye staining prevalent throughout the right hemisphere of the

brain, ipsilateral to mannitol perfusion, provided qualitative evidence confirming effective

and extensive BBB disruption. This data was combined with studies of ADC and

histological changes in order to further characterize the edema.

Apparent Diffusion Coefficient Map Analysis

Both echo planar based spin echo (EPI) and spin echo (SE) diffusion weighted

imaging (DWI) data was collected on rats, 1 hour after mannitol delivery. ADC data

generated from this data did not show differences between the two types of imaging to be

Figure 7-1. Diagram comparing Gd-DTPA infusion distribution in normal tissue to edema formation from mannitol in similar regions. **A:** T1 quantitative map image of Gd-DTPA at end of infusion in forebrain cortical gray matter of normal brain. Note that the area of Gd-DTPA distribution is shown as darker than adjacent tissue due to the decrease in T1 value caused by the Gd relaxivity effect. **B:** Post-processed outline of T1 Map depicting Gd-DTPA at end of infusion in deep gray matter (caudate/putamen) of normal brain (image courtesy of P. Haar[3]). **C:** Edema formation seen in forebrain cortical gray matter, 1 hour after mannitol infusion. **D:** Edema formation seen in deep gray matter (caudate/putamen), 1 hour after mannitol infusion.
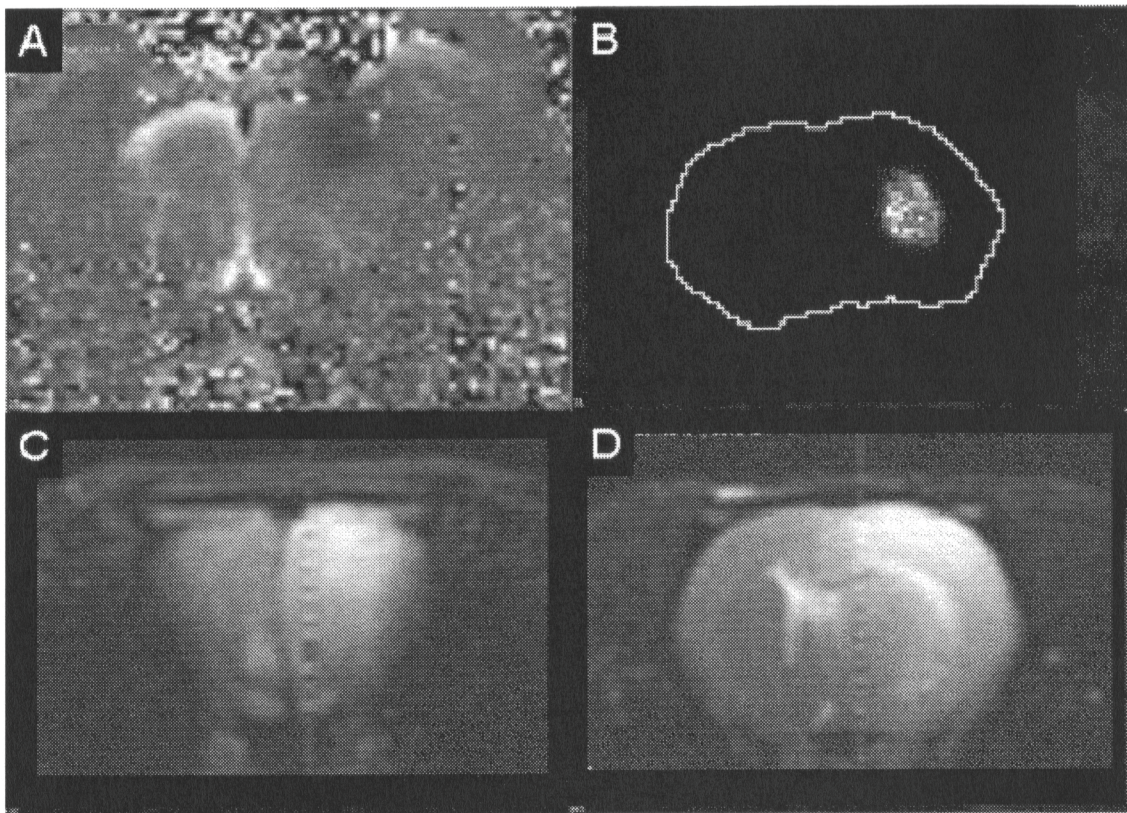
statistically different. ADC response was therefore studied based on EPI DWI alone as it was a faster technique and more time-points could be collected.

VE has been shown to cause an elevation in ADC values, while CE can cause a lowering of ADC. [9] Therefore, we would expect to see an elevation of ADC in the regions of observed edema in order to characterize the presence of VE. Based on our results, the average gray matter ADC values were lower in both hemispheres during the first hour of edema formation, although these values were not significantly different from normal values. Because a large amount of edema was present at this time point, based on T2 and f_w analysis, we would have expected ADC values to have been affected more significantly, and in the opposite direction than the small, non-significant decrease that was observed. This was the first indicator that our model may have contained both CE and VE components in the acute phase, thereby pseudonormalizing ADC values. The right hemisphere gray matter ADC was slightly but non-significantly higher than the left hemisphere after 1 hour and significantly so after 24 hours. At the 24-hour mark, the right hemisphere exhibited ADC values that were statistically significantly higher than normal tissue. This would be consistent with the presence of some VE effect in that hemisphere, in corroboration with the hyperintensity observed in T2W images at the 24 hour time point. Given these findings, we went on to perform histological examination of the edematous tissue to further investigate these possibilities.

Microscopy Analysis

After light microscopy (LM) examination, there appeared to be some cytotoxic effect observed in the edematous gray matter under H&E staining. Studies have found that cytotoxicity is observed by shrunken neurons with perineuronal spaces,[9] we observed in the edematous hemispheres 2 hours post mannitol delivery. Previous studies have also shown similar spongy appearance in the neuropil and the appearance of shrunken neurons after a single bolus of mannitol perfusion in the rat brain, using the same rate and dose used in the current study.[136] The spongy appearance of the neuropil and perivascular spaces seen under H&E have also been also observed in other edematous tissue where BBB disruption occurred.[142;149]

Our histological studies with H&E staining drew concern for injury to cells, with the majority of neurons in the perfused gray matter appearing as shrunken and dark in appearance, but transmission electron microscopy (TEM) failed to show significant evidence of injury to these shrunken neurons. The nucleus of the neurons in the edematous tissue appeared healthy, in addition to the presence of healthy-appearing mitochondria observed in the cytoplasm. Therefore, the neurons in the mannitol perfused-hemisphere appear to have been in a healthy state at the moment of fixation for EM, but the presence of swollen processes surrounding the neurons suggest the possibility that these cells could be in a beginning phase of degeneration.[137] The perineuronal space appeared to be expanded cellular processes surrounding the neuron, and may have contributed to the shrunken appearance of the neurons, whereby processes pushed into the cytoplasm to create a scalloped appearance. This may have helped to account for the darker appearance

of these neurons in the paraffin embedded LM studies as the cytoplasm was being compacted. TEM also revealed the perivascular spaces seen under H&E to be swollen cellular processes, as opposed to expanded ECS, mostly likely belonging to astrocytes. Swollen astrocytic processes surrounding the blood vessels indicate some BBB disruption to have occurred[142] as was confirmed earlier by EB dye. The fluid leaking into the ECS may have caused hypertonic conditions that could have withdrawn water from the neuron's cytoplasm, contributing to neuronal shrinkage. The spongy appearance of the neuropil observed in edematous regions under H&E appeared to be due to the swollen cellular processes, in addition to putative expansion of ECS. This would indicate an increase in both intracellular and extracellular fluid, thereby presenting the possibility of ADC effects from the former counteracting with ADC effects from the latter. Further studies would need to be conducted to verify that ECS expansion was indeed occurring.

EB dye in conjunction with perivascular spaces observed under LM and TEM revealed BBB disruption, while swollen processes surrounding shrunken neurons suggest the presence of mild neurotoxic effects. When examined with our MRI results, the edema appears to result from some sort of combination of VE and CE in the acute phase, while later (at 24 hours) VE appears to be a dominant portion as evidenced by raised ADC. This argues that the edema seen is not a "pure" example of vasogenic effect, but represents a combination of VE due to BBB disruption followed by possible cytotoxic effects.

Conclusion

Based on our results, our starting hypothesis did not prove all together true; three infusions of 25% mannitol did not produce conditions of "pure" VE. We conclude that there is an acute phase of extensive edema, which seems to be a mixture of CE and VE, which have may a pseudo-normalization effect on the ADC values. The acute edema formed within an hour after mannitol infusion was consistent and widespread throughout the cortical and deep gray region, and had microscopic and ultrastructural features similar to other classic studies of brain edema. We also conclude that this model is applicable for CED study in edematous conditions, albeit not in a setting of purely VE.

The triple mannitol infusion model for edema presented and characterized in this study provides a good starting point for further investigations that may lead to a purer model of VE. Due to the high mortality, the current model is not robust enough to allow for animal survival to enable studies of edema resolution and longer-term consequences of the mannitol infusions. Therefore, further studies will need to investigate changes in mannitol dosage that are titrated to changes in ADC values and water content changes, and not to T2 changes alone, as were used in the development of this initial model. Indeed, further studies have already been initiated, in which early results demonstrate a reduced mortality with decreased doses and volumes of mannitol infusion. These results are promising for subsequent MRI investigations.

Literature Cited

Reference List

1. Chen MY, Chen ZJ, Gillies GT, Haar PJ, Broaddus WC. Intratumoral Administration and Convection-Enhanced Delivery. In: Newton HB (ed) *Handbook of Brain Tumor Chemotherapy*. Amsterdam: Elsevier, 2006.

2. Milhorat TH, Johnson WD, Dow-Edwards DL. Relationship between oedema, blood pressure, and blood flow following local brain injury. *Neurol.Res.* 1989:**11**: 29-32.

3. Haar, P. Quantifying and Modeling Convection-Enhanced Delivery in Pathological Brain States. 2005. 12-1-2004.
   Ref Type: Thesis/Dissertation

4. Barzo P, Marmarou A, Fatouros P, Hayasaki K, Corwin F. Contribution of vasogenic and cellular edema to traumatic brain swelling measured by diffusion-weighted imaging. *J Neurosurg.* 1997:**87**: 900-907.

5. Marmarou A, Portella G, Barzo P *et al.* Distinguishing between cellular and vasogenic edema in head injured patients with focal lesions using magnetic resonance imaging. *Acta Neurochir.Suppl* 2000:**76**: 349-351.

6. Klatzo I. Disturbances of the blood-brain barrier in cerebrovascular disorders. *Acta Neuropathol.Suppl (Berl)* 1983:**8**: 81-88.

7. Loubinoux I, Volk A, Borredon J *et al.* Spreading of vasogenic edema and cytotoxic edema assessed by quantitative diffusion and T2 magnetic resonance imaging. *Stroke* 1997:**28**: 419-426.

8. Thapar K, Taylor MD, Laws ER, Rutka JT. Brain edema, increased intracranial pressure, and vascular effects of human brain tumors. In: Kaye AH, Laws ER (eds) *Brain Tumors - An Encyclopedic Approach*. Churchill Livingston, 2001.

9. Ito J, Marmarou A, Barzo P, Fatouros P, Corwin F. Characterization of edema by diffusion-weighted imaging in experimental traumatic brain injury. *J Neurosurg.* 1996:**84**: 97-103.

10. Graeber MB, Blakemore WF, Kreutzberg GW. Cellular pathology of the central nervous system. In: Graham DI, Lantos PL (eds) *Greenfield's Neuropathology*. London: Arnold, 2002.

11. Barzo P, Marmarou A, Fatouros P, Corwin F, Dunbar J. Magnetic resonance imaging-monitored acute blood-brain barrier changes in experimental traumatic brain injury. *J Neurosurg.* 1996:**85**: 1113-1121.

12. Loubinoux I, Volk A, Borredon J *et al.* Spreading of vasogenic edema and cytotoxic edema assessed by quantitative diffusion and T2 magnetic resonance imaging. *Stroke* 1997:**28**: 419-426.

13. Dublin WB. Tumors. *Fundamentals of Neuropathology.* Springfield: Charles C Thomas, 1954.

14. Cloughesy TF, Black KL. Peritumoral edema. In: Berger MS, Wilson CB (eds) *The gliomas.* Philadelphia: W.B. Saunders Company, 1999.

15. Henson JW. Treatment of glioblastoma multiforme: a new standard. *Arch.Neurol.* 2006:**63**: 337-341.

16. Maher EA, Furnari FB, Bachoo RM *et al.* Malignant glioma: genetics and biology of a grave matter. *Genes Dev.* 2001:**15**: 1311-1333.

17. Reardon DA, Wen PY. Therapeutic advances in the treatment of glioblastoma: rationale and potential role of targeted agents. *Oncologist.* 2006:**11**: 152-164.

18. Qureshi NH, Bankiewicz KS, Louis DN, Hochberg FH, Chiocca EA, Harsh GR. Multicolumn infusion of gene therapy cells into human brain tumors: technical report. *Neurosurgery* 2000:**46**: 663-668.

19. Ohgaki H, Dessen P, Jourde B *et al.* Genetic pathways to glioblastoma: a population-based study. *Cancer Res.* 2004:**64**: 6892-6899.

20. Lantos PL, Luthert PJ, Deane BR. Vascular permeability and cerebral oedema in experimental brain tumors. In: Inaba Y, Klatzo I, Spatz M (eds) *Brain edema.* Berlin: Springer-Verlag, 1985.

21. Kroll RA, Neuwelt EA. Outwitting the blood-brain barrier for therapeutic purposes: osmotic opening and other means. *Neurosurgery* 1998:**42**: 1083-1099.

22. Broaddus WC, Gillies GT, Lamfers ML. Image-guided intraparenchymal drug and cell delivery. In: Latchaw R, Kucharczyk J, Moseley M (eds) *Imaging of the Nervous System: Diagnostic and Therapeutic Applications.* Philadelphia: Elsevier Mosby, 2005.

23. Gillies GT, Smith JH, Humphrey JA, Broaddus WC. Positive pressure infusion of therapeutic agents into brain tissues: mathematical and experimental simulations. *Technol.Health Care* 2005:**13**: 235-243.

24. Oldfield E, Broaddus WC, Trask T *et al.* Phase II trial of convection-enhanced distribution of recombinant immunotoxin in patients with recurrent malignant gliomas. *American Association of Neurological Surgeons, Annual Meeting, San Francisco, CA* 2000.

25. Mardor Y, Roth Y, Lidar Z *et al.* Monitoring response to convection-enhanced taxol delivery in brain tumor patients using diffusion-weighted magnetic resonance imaging. *Cancer Res.* 2001:**61**: 4971-4973.

26. Prabhu SS, Broaddus WC, Gillies GT, Loudon WG, Chen ZJ, Smith B. Distribution of macromolecular dyes in brain using positive pressure infusion: a model for direct controlled delivery of therapeutic agents. *Surg.Neurol.* 1998:**50**: 367-375.

27. Bobo RH, Laske DW, Akbasak A, Morrison PF, Dedrick RL, Oldfield EH. Convection-enhanced delivery of macromolecules in the brain. *Proc.Natl.Acad.Sci.U.S.A* 1994:**91**: 2076-2080.

28. Broaddus WC, Prabhu SS, Gillies GT *et al.* Distribution and stability of antisense phosphorothioate oligonucleotides in rodent brain following direct intraparenchymal controlled-rate infusion. *J.Neurosurg.* 1998:**88**: 734-742.

29. Broaddus WC, Prabhu SS Wu-Pong S Gillies GT Fillmore HL. Strategies for the Design and Delivery of Antisense Oligonucleotide in Central Nervous System. Meth.Enzymol.Antisen.Technol.(Part.B: Applications).314:121-135. 2000.
Ref Type: Generic

30. Hall WA, Flores EP, Low WC. Antisense oligonucleotides for central nervous system tumors. *Neurosurgery* 1996:**38**: 376-383.

31. Chiocca EA, Broaddus WC, Gillies GT, Visted T, Lamfers ML. Neurosurgical delivery of chemotherapeutics, targeted toxins, genetic and viral therapies in neuro-oncology. *J.Neurooncol.* 2004:**69**: 101-117.

32. Dodson RF, Tagashira Y, Kawamura Y, Chu LW. Morphological responses of cerebral tissues to temporary ischemia. *Can.J Neurol Sci.* 1975:**2**: 173-177.

33. Avendano C, Roda JM, Carceller F, Diez-Tejedor E. Morphometric study of focal cerebral ischemia in rats: a stereological evaluation. *Brain Res* 1995:**673**: 83-92.

34. Pierpaoli C, Righini A, Linfante IT-CJH, Alger JR, Chiro G. Histopathologic correlates of abnormal water diffusion in cerebral ischemia: diffusion-weighted MR imaging and light and electron microscopic study. *Radiology* 1993:**189**: 439-448.

35. Sykova E. Diffusion barriers evoked by cell swelling, astrogliosis and pathological states in the CNS. *Journal of Physiology* 1998:**511P**: 8S.

36. Sykova E, Mazel T, Vargova L, Vorisek I, Prokopova-Kubinova S. Extracellular space diffusion and pathological states. *Prog.Brain Res.* 2000:**125**: 155-178.

37. Kaal EC, Vecht CJ. The management of brain edema in brain tumors. *Curr.Opin.Oncol.* 2004:**16**: 593-600.

38. Vinas FC, Dujovny M, Hodgkinson D. Early hemodynamic changes at the microcirculatory level and effects of mannitol following focal cryogenic injury. *Neurol.Res.* 1995:**17**: 465-468.

39. Liebner S, Fischmann A, Rascher G *et al.* Claudin-1 and claudin-5 expression and tight junction morphology are altered in blood vessels of human glioblastoma multiforme. *Acta Neuropathol.(Berl)* 2000:**100**: 323-331.

40. Papadopoulos MC, Saadoun S, Woodrow CJ *et al.* Occludin expression in microvessels of neoplastic and non-neoplastic human brain. *Neuropathol.Appl.Neurobiol.* 2001:**27**: 384-395.

41. Huber JD, Egleton RD, Davis TP. Molecular physiology and pathophysiology of tight junctions in the blood-brain barrier. *Trends Neurosci.* 2001:**24**: 719-725.

42. Abbruscato TJ, Davis TP. Protein expression of brain endothelial cell E-cadherin after hypoxia/aglycemia: influence of astrocyte contact. *Brain Res.* 1999:**842**: 277-286.

43. Engelhard HH, Groothuis DG. The blood brain barrier: structure, function, and response to neoplasia. In: Berger MS, Wilson CB (eds) *The gliomas*. Philadelphia: W.B. Saunders Company, 1999.

44. Betz AL, Keep RF, Beer ME, Ren XD. Blood-brain barrier permeability and brain concentration of sodium, potassium, and chloride during focal ischemia. *J.Cereb.Blood Flow Metab* 1994:**14**: 29-37.

45. Stevenson BR, Begg DA. Concentration-dependent effects of cytochalasin D on tight junctions and actin filaments in MDCK epithelial cells. *J.Cell Sci.* 1994:**107** (**Pt 3**): 367-375.

46. Stevenson BR, Begg DA. Concentration-dependent effects of cytochalasin D on tight junctions and actin filaments in MDCK epithelial cells. *J.Cell Sci.* 1994:**107** (**Pt 3**): 367-375.

47. Wachtel M, Frei K, Ehler E, Fontana A, Winterhalter K, Gloor SM. Occludin proteolysis and increased permeability in endothelial cells through tyrosine phosphatase inhibition. *J.Cell Sci.* 1999:**112 (Pt 23)**: 4347-4356.

48. Bolton SJ, Anthony DC, Perry VH. Loss of the tight junction proteins occludin and zonula occludens-1 from cerebral vascular endothelium during neutrophil-induced blood-brain barrier breakdown in vivo. *Neuroscience* 1998:**86**: 1245-1257.

49. Abbott NJ. Inflammatory mediators and modulation of blood-brain barrier permeability. *Cell Mol.Neurobiol.* 2000:**20**: 131-147.

50. Wang W, Dentler WL, Borchardt RT. VEGF increases BMEC monolayer permeability by affecting occludin expression and tight junction assembly. *Am.J.Physiol Heart Circ.Physiol* 2001:**280**: H434-H440.

51. Black KL, Ningaraj NS. Modulation of brain tumor capillaries for enhanced drug delivery selectively to brain tumor. *Cancer Control* 2004:**11**: 165-173.

52. Farkas A, Szatmari E, Orbok A *et al.* Hyperosmotic mannitol induces Src kinase-dependent phosphorylation of beta-catenin in cerebral endothelial cells. *J.Neurosci.Res.* 2005:**80**: 855-861.

53. Rapoport SI. Osmotic opening of the blood-brain barrier: principles, mechanism, and therapeutic applications. *Cell Mol.Neurobiol.* 2000:**20**: 217-230.

54. Muldoon LL, Pagel MA, Kroll RA, Roman-Goldstein S, Jones RS, Neuwelt EA. A physiological barrier distal to the anatomic blood-brain barrier in a model of transvascular delivery. *AJNR Am.J.Neuroradiol.* 1999:**20**: 217-222.

55. Turski PA, Perman WH, Hald JK, Houston LW, Strother CM, Sackett JF. Clinical and experimental vasogenic edema: in vivo sodium MR imaging. Work in progress. *Radiology* 1986:**160**: 821-825.

56. Pan GY, Liu XD, Liu GQ. Intracarotid infusion of hypertonic mannitol changes permeability of blood-brain barrier to methotrexate in rats. *Acta Pharmacol.Sin.* 2000:**21**: 613-616.

57. Kaya M, Gulturk S, Elmas I *et al.* The effects of magnesium sulfate on blood-brain barrier disruption caused by intracarotid injection of hyperosmolar mannitol in rats. *Life Sci.* 2004:**76**: 201-212.

58. Lin TN, He YY, Wu G, Khan M, Hsu CY. Effect of brain edema on infarct volume in a focal cerebral ischemia model in rats. *Stroke* 1993:**24**: 117-121.

59. Paczynski RP, He YY, Diringer MN, Hsu CY. Multiple-dose mannitol reduces brain water content in a rat model of cortical infarction. *Stroke* 1997:**28**: 1437-1443.

60. Marmarou A, Tanaka K, Shulman K. An improved gravimetric measure of cerebral edema. *J.Neurosurg.* 1982:**56**: 246-253.

61. Fatouros PP, Marmarou A. Use of magnetic resonance imaging for in vivo measurements of water content in human brain: method and normal values. *J.Neurosurg.* 1999:**90**: 109-115.

62. Baskaya MK, Rao AM, Dogan A, Donaldson D, Dempsey RJ. The biphasic opening of the blood-brain barrier in the cortex and hippocampus after traumatic brain injury in rats. *Neurosci.Lett.* 1997:**226**: 33-36.

63. Baskaya MK, Rao AM, Prasad MR, Dempsey RJ. Regional activity of ornithine decarboxylase and edema formation after traumatic brain injury. *Neurosurgery* 1996:**38**: 140-145.

64. Lin TN, He YY, Wu G, Khan M, Hsu CY. Effect of brain edema on infarct volume in a focal cerebral ischemia model in rats. *Stroke* 1993:**24**: 117-121.

65. Schwarcz A, Berente Z, Osz E, Doczi T. In vivo water quantification in mouse brain at 9.4 Tesla in a vasogenic edema model. *Magn Reson.Med.* 2001:**46**: 1246-1249.

66. Lin TN, He YY, Wu G, Khan M, Hsu CY. Effect of brain edema on infarct volume in a focal cerebral ischemia model in rats. *Stroke* 1993:**24**: 117-121.

67. Baskaya MK, Rao AM, Prasad MR, Dempsey RJ. Regional activity of ornithine decarboxylase and edema formation after traumatic brain injury. *Neurosurgery* 1996:**38**: 140-145.

68. Baskaya MK, Rao AM, Dogan A, Donaldson D, Dempsey RJ. The biphasic opening of the blood-brain barrier in the cortex and hippocampus after traumatic brain injury in rats. *Neurosci.Lett.* 1997:**226**: 33-36.

69. Fatouros PP, Marmarou A. Use of magnetic resonance imaging for in vivo measurements of water content in human brain: method and normal values. *J.Neurosurg.* 1999:**90**: 109-115.

70. Baskaya MK, Rao AM, Prasad MR, Dempsey RJ. Regional activity of ornithine decarboxylase and edema formation after traumatic brain injury. *Neurosurgery* 1996:**38**: 140-145.

71. Fatouros PP, Marmarou A. Use of magnetic resonance imaging for in vivo measurements of water content in human brain: method and normal values. *J.Neurosurg.* 1999:**90**: 109-115.

72. Baskaya MK, Rao AM, Prasad MR, Dempsey RJ. Regional activity of ornithine decarboxylase and edema formation after traumatic brain injury. *Neurosurgery* 1996:**38**: 140-145.

73. Fatouros PP, Marmarou A. Use of magnetic resonance imaging for in vivo measurements of water content in human brain: method and normal values. *J.Neurosurg.* 1999:**90**: 109-115.

74. Fujiwara K, Nitsch C, Suzuki R, Klatzo I. Factors in the reproducibility of the gravimetric method for evaluation of edematous changes in the brain. *Neurol.Res.* 1981:**3**: 345-361.

75. Fatouros PP, Marmarou A. Use of magnetic resonance imaging for in vivo measurements of water content in human brain: method and normal values. *J.Neurosurg.* 1999:**90**: 109-115.

76. Marmarou A, Fatouros P, Ward J, Appley A, Young H. In vivo measurement of brain water by MRI. *Acta Neurochir.Suppl (Wien.)* 1990:**51**: 123-124.

77. Fatouros PP, Marmarou A. Use of magnetic resonance imaging for in vivo measurements of water content in human brain: method and normal values. *J Neurosurg.* 1999:**90**: 109-115.

78. Loubinoux I, Volk A, Borredon J *et al.* Spreading of vasogenic edema and cytotoxic edema assessed by quantitative diffusion and T2 magnetic resonance imaging. *Stroke* 1997:**28**: 419-426.

79. Fatouros PP, Marmarou A. Use of magnetic resonance imaging for in vivo measurements of water content in human brain: method and normal values. *J.Neurosurg.* 1999:**90**: 109-115.

80. Loubinoux I, Volk A, Borredon J *et al.* Spreading of vasogenic edema and cytotoxic edema assessed by quantitative diffusion and T2 magnetic resonance imaging. *Stroke* 1997:**28**: 419-426.

81. Fatouros PP, Marmarou A. Use of magnetic resonance imaging for in vivo measurements of water content in human brain: method and normal values. *J.Neurosurg.* 1999:**90**: 109-115.

82. Fatouros PP, Marmarou A, Kraft KA, Inao S, Schwarz FP. In vivo brain water determination by T1 measurements: effect of total water content, hydration fraction, and field strength. *Magn Reson.Med.* 1991:**17**: 402-413.

83. Fatouros PP, Marmarou A. Use of magnetic resonance imaging for in vivo measurements of water content in human brain: method and normal values. *J.Neurosurg.* 1999:**90**: 109-115.

84. Fatouros PP, Marmarou A. Use of magnetic resonance imaging for in vivo measurements of water content in human brain: method and normal values. *J.Neurosurg.* 1999:**90**: 109-115.

85. Fatouros PP, Marmarou A. Use of magnetic resonance imaging for in vivo measurements of water content in human brain: method and normal values. *J.Neurosurg.* 1999:**90**: 109-115.

86. Fatouros PP, Marmarou A. Use of magnetic resonance imaging for in vivo measurements of water content in human brain: method and normal values. *J.Neurosurg.* 1999:**90**: 109-115.

87. Fatouros PP, Marmarou A. Use of magnetic resonance imaging for in vivo measurements of water content in human brain: method and normal values. *J.Neurosurg.* 1999:**90**: 109-115.

88. Duong TQ, Sehy JV, Yablonskiy DA, Snider BJ, Ackerman JJ, Neil JJ. Extracellular apparent diffusion in rat brain. *Magn Reson.Med.* 2001:**45**: 801-810.

89. Matsumoto K, Lo EH, Pierce AR, Wei H, Garrido L, Kowall NW. Role of vasogenic edema and tissue cavitation in ischemic evolution on diffusion-weighted imaging: comparison with multiparameter MR and immunohistochemistry. *AJNR Am.J.Neuroradiol.* 1995:**16**: 1107-1115.

90. Matsumoto K, Lo EH, Pierce AR, Wei H, Garrido L, Kowall NW. Role of vasogenic edema and tissue cavitation in ischemic evolution on diffusion-weighted imaging: comparison with multiparameter MR and immunohistochemistry. *AJNR Am.J.Neuroradiol.* 1995:**16**: 1107-1115.

91. Fatouros PP, Marmarou A. Use of magnetic resonance imaging for in vivo measurements of water content in human brain: method and normal values. *J.Neurosurg.* 1999:**90**: 109-115.

92. Matsumoto K, Lo EH, Pierce AR, Wei H, Garrido L, Kowall NW. Role of vasogenic edema and tissue cavitation in ischemic evolution on diffusion-weighted imaging: comparison with multiparameter MR and immunohistochemistry. *AJNR Am.J.Neuroradiol.* 1995:**16**: 1107-1115.

93. Weidauer S, Ziemann U, Thomalske C, Gaa J, Lanfermann H, Zanella FE. Vasogenic edema in Bickerstaff's brainstem encephalitis: a serial MRI study. *Neurology* 2003:**61**: 836-838.

94. Papadopoulos MC, Manley GT, Krishna S, Verkman AS. Aquaporin-4 facilitates reabsorption of excess fluid in vasogenic brain edema. *FASEB J.* 2004:**18**: 1291-1293.

95. Cosolo WC, Martinello P, Louis WJ, Christophidis N. Blood-brain barrier disruption using mannitol: time course and electron microscopy studies. *Am.J.Physiol* 1989:**256**: R443-R447.

96. Papadopoulos MC, Binder DK, Verkman AS. Enhanced macromolecular diffusion in brain extracellular space in mouse models of vasogenic edema measured by cortical surface photobleaching. *FASEB J.* 2005:**19**: 425-427.

97. Kim HJ, Pyeun YS, Kim YW *et al.* A model for research on the blood-brain barrier disruption induced by unsaturated fatty acid emulsion. *Invest Radiol.* 2005:**40**: 270-276.

98. Hirano A, Marmarou A, Nakamura T, Inoue A. The fine structural study of brain response to intracerebral infusion of serum in the cat. In: Inaba Y, Klatzo I, Spatz M (eds) *Brain edema*. Berlin: Springer-Verlag, 1985.

99. Ohata K, Marmarou A, Povlishock JT. An immunocytochemical study of protein clearance in brain infusion edema. *Acta Neuropathol.(Berl)* 1990:**81**: 162-177.

100. Ohata K, Marmarou A. Clearance of brain edema and macromolecules through the cortical extracellular space. *J Neurosurg.* 1992:**77**: 387-396.

101. Ohata K, Marmarou A, Povlishock JT. Immunocytochemical studies of oedema protein clearance in the rat. *Acta Neurochir.Suppl (Wien.)* 1990:**51**: 93-95.

102. Marmarou A, Tanaka K, Shulman K. The brain response to infusion edema: dynamics of fluid resolution. In: Hartmann A, Brock M (eds) *Treatment of cerebral edema*. Berlin: Springer-Verlag, 1982.

103. Jansen O, Hartmann M, Gass P, Sartor K. [Magnetic resonance tomography of vasogenic brain edema in animal experiments]. *Rofo* 1996:**164**: 406-412.

104. Fazekas A, Komoly S. Specific demonstration of albumin by immunohistological techniques in human vasogenic brain edema. *Acta Neuropathol.Suppl (Berl)* 1981:**7**: 70-72.

105. Groger U, Marmarou A. Importance of protein content in the edema fluid for the resolution of brain edema. *Adv.Neurol.* 1990:**52**: 215-218.

106. Wrba E, Nehring V, Baethmann A, Reulen HJ, Uhl E. Resolution of experimental vasogenic brain edema at different intracranial pressures. *Acta Neurochir.Suppl (Wien.)* 1998:**71**: 313-315.

107. Ghabriel MN, Zhu C, Reilly PL, Blumbergs PC, Manavis J, Finnie JW. Toxin-induced vasogenic cerebral oedema in a rat model. *Acta Neurochir.Suppl* 2000:**76**: 231-236.

108. Gardenfors A, Nilsson F, Skagerberg G, Ungerstedt U, Nordstrom CH. Cerebral physiological and biochemical changes during vasogenic brain oedema induced by intrathecal injection of bacterial lipopolysaccharides in piglets. *Acta Neurochir.(Wien.)* 2002:**144**: 601-608.

109. Houkin K, Abe H, Hashiguchi Y, Seri S. Magnetic resonance imaging of cold injury-induced brain edema in rats. *Neurol.Med.Chir (Tokyo)* 1996:**36**: 72-77.

110. Bodsch W, Hurter T, Hossmann KA. Immunochemical method for quantitative evaluation of vasogenic brain edema following cold injury of rat brain. *Brain Res.* 1982:**249**: 111-121.

111. Houkin K, Abe H, Hashiguchi Y, Seri S. Magnetic resonance imaging of cold injury-induced brain edema in rats. *Neurol.Med.Chir (Tokyo)* 1996:**36**: 72-77.

112. Houkin K, Abe H, Hashiguchi Y, Seri S. Magnetic resonance imaging of cold injury-induced brain edema in rats. *Neurol.Med.Chir (Tokyo)* 1996:**36**: 72-77.

113. Bodsch W, Hurter T, Hossmann KA. Immunochemical method for quantitative evaluation of vasogenic brain edema following cold injury of rat brain. *Brain Res.* 1982:**249**: 111-121.

114. Houkin K, Abe H, Hashiguchi Y, Seri S. Magnetic resonance imaging of cold injury-induced brain edema in rats. *Neurol.Med.Chir (Tokyo)* 1996:**36**: 72-77.

115. Bodsch W, Hurter T, Hossmann KA. Immunochemical method for quantitative evaluation of vasogenic brain edema following cold injury of rat brain. *Brain Res.* 1982:**249**: 111-121.

116. Houkin K, Abe H, Hashiguchi Y, Seri S. Magnetic resonance imaging of cold injury-induced brain edema in rats. *Neurol.Med.Chir (Tokyo)* 1996:**36**: 72-77.

117. Bodsch W, Hurter T, Hossmann KA. Immunochemical method for quantitative evaluation of vasogenic brain edema following cold injury of rat brain. *Brain Res.* 1982:**249**: 111-121.

118. Baker RN, Cancilla PA, Pollock PS, Frommes SP. The movement of exogenous protein in experimental cerebral edema. An electron microscopic study after freeze-injury. *J.Neuropathol.Exp.Neurol.* 1971:**30**: 668-679.

119. Go KG, Zijlstra WG, Flanderijn H, Zuiderveen F. Circulatory factors influencing exudation in cold-induced cerebral edema. *Exp.Neurol.* 1974:**42**: 332-338.

120. Stoffel M, Blau C, Reinl H *et al.* Identification of brain tissue necrosis by MRI: validation by histomorphometry. *J.Neurotrauma* 2004:**21**: 733-740.

121. Houkin K, Abe H, Hashiguchi Y, Seri S. Magnetic resonance imaging of cold injury-induced brain edema in rats. *Neurol.Med.Chir (Tokyo)* 1996:**36**: 72-77.

122. Houkin K, Abe H, Hashiguchi Y, Seri S. Magnetic resonance imaging of cold injury-induced brain edema in rats. *Neurol.Med.Chir (Tokyo)* 1996:**36**: 72-77.

123. Vinas FC, Dujovny M, Hodgkinson D. Early hemodynamic changes at the microcirculatory level and effects of mannitol following focal cryogenic injury. *Neurol.Res.* 1995:**17**: 465-468.

124. Bodsch W, Hurter T, Hossmann KA. Immunochemical method for quantitative evaluation of vasogenic brain edema following cold injury of rat brain. *Brain Res.* 1982:**249**: 111-121.

125. Bodsch W, Hurter T, Hossmann KA. Immunochemical method for quantitative evaluation of vasogenic brain edema following cold injury of rat brain. *Brain Res.* 1982:**249**: 111-121.

126. Houkin K, Abe H, Hashiguchi Y, Seri S. Magnetic resonance imaging of cold injury-induced brain edema in rats. *Neurol.Med.Chir (Tokyo)* 1996:**36**: 72-77.

127. Houkin K, Abe H, Hashiguchi Y, Seri S. Magnetic resonance imaging of cold injury-induced brain edema in rats. *Neurol.Med.Chir (Tokyo)* 1996:**36**: 72-77.

128. Pan GY, Liu XD, Liu GQ. Intracarotid infusion of hypertonic mannitol changes permeability of blood-brain barrier to methotrexate in rats. *Acta Pharmacol.Sin.* 2000:**21**: 613-616.

129. Ikeda M, Bhattacharjee AK, Kondoh T, Nagashima T, Tamaki N. Synergistic effect of cold mannitol and Na(+)/Ca(2+) exchange blocker on blood-brain barrier opening. *Biochem.Biophys.Res.Commun.* 2002:**291**: 669-674.

130. Kaufmann AM, Cardoso ER. Aggravation of vasogenic cerebral edema by multiple-dose mannitol. *J.Neurosurg.* 1992:**77**: 584-589.

131. Battison C, Andrews PJ, Graham C, Petty T. Randomized, controlled trial on the effect of a 20% mannitol solution and a 7.5% saline/6% dextran solution on increased intracranial pressure after brain injury. *Crit Care Med.* 2005:**33**: 196-202.

132. Schrot RJ, Muizelaar JP. Sugar or salt? *Crit Care Med.* 2005:**33**: 257-258.

133. Vinas FC, Dujovny M, Hodgkinson D. Early hemodynamic changes at the microcirculatory level and effects of mannitol following focal cryogenic injury *Neurol.Res.* 1995:**17**: 465-468.

134. Schrot RJ, Muizelaar JP. Sugar or salt? *Crit Care Med.* 2005:**33**: 257-258.

135. Schrot RJ, Muizelaar JP. Sugar or salt? *Crit Care Med.* 2005:**33**: 257-258.

136. Salahuddin TS, Johansson BB, Kalimo H, Olsson Y. Structural changes in the rat brain after carotid infusions of hyperosmolar solutions: a light microscopic and immunohistochemical study. *Neuropathol.Appl.Neurobiol.* 1988:**14**: 467-482.

137. Salahuddin TS, Johansson BB, Kalimo H, Olsson Y. Structural changes in the rat brain after carotid infusions of hyperosmolar solutions. An electron microscopic study. *Acta Neuropathol.(Berl)* 1988:**77**: 5-13.

138. Pan GY, Liu XD, Liu GQ. Intracarotid infusion of hypertonic mannitol changes permeability of blood-brain barrier to methotrexate in rats. *Acta Pharmacol.Sin.* 2000:**21**: 613-616.

139. Pan GY, Liu XD, Liu GQ. Intracarotid infusion of hypertonic mannitol changes permeability of blood-brain barrier to methotrexate in rats. *Acta Pharmacol.Sin.* 2000:**21**: 613-616.

140. Weller RO, Swash M, McLellan DL, Scholtz CL. *Clinical Neuropathology.* Berlin: Springer-Verlag, 1983.

141. Kimura R, Nakase H, Tamaki R, Sakaki T. Vascular endothelial growth factor antagonist reduces brain edema formation and venous infarction. *Stroke* 2005:**36**: 1259-1263.

142. Weller RO, Swash M, McLellan DL, Scholtz CL. General Pathology of the Central Nervous System. *Clinical Neuropathology.* Berlin: Springer-Verlag, 1983.

143. Pan GY, Liu XD, Liu GQ. Intracarotid infusion of hypertonic mannitol changes permeability of blood-brain barrier to methotrexate in rats. *Acta Pharmacol.Sin.* 2000:**21**: 613-616.

144. Li F, Liu KF, Silva MD *et al.* Transient and permanent resolution of ischemic lesions on diffusion-weighted imaging after brief periods of focal ischemia in rats : correlation with histopathology. *Stroke* 2000:**31**: 946-954.

145. Fatouros PP, Marmarou A. Use of magnetic resonance imaging for in vivo measurements of water content in human brain: method and normal values. *J.Neurosurg.* 1999:**90**: 109-115.

146. Fatouros PP, Marmarou A, Kraft KA, Inao S, Schwarz FP. In vivo brain water determination by T1 measurements: effect of total water content, hydration fraction, and field strength. *Magn Reson.Med.* 1991:**17**: 402-413.

147. Go KG, Zijlstra WG, Flanderijn H, Zuiderveen F. Circulatory factors influencing exudation in cold-induced cerebral edema. *Exp.Neurol.* 1974:**42**: 332-338.

148. Fatouros PP, Marmarou A. Use of magnetic resonance imaging for in vivo measurements of water content in human brain: method and normal values. *J.Neurosurg.* 1999:**90**: 109-115.

149. Perret GE, Kernohan JW. Histopathological changes of the brain caused by intracranial tumors (so-called edema or swelling of the brain). *J.Neuropath.& Exper.Neurol.* 1943:**2**: 341-352.

VITA

Anshu Shukla was born on January 19th, 1980 in Varanasi, India and is an Indian citizen residing as a Permanent Resident in the United States. He graduated with honors from Oakton High School in Vienna, Virginia in 1998. He matriculated into Duke University where he completed a triple major in Biomedical Engineering, Electrical Engineering and Economics. He graduated from Duke University with a Bachelor of Sciences in Engineering in 2002.

After college, he pursued business experiences in the financial world through a Leadership Development Program at J.P. Morgan Chase. In 2003, he became a Business Analyst with Accenture, an IT consulting firm, and moved on to specialize as a Data Quality Analyst at America Online, Inc in 2004. After gaining a rewarding experience in the corporate world, Anshu returned to academics and completed a Certificate in Anatomy and Neurobiology at Virginia Commonwealth School of Medicine in 2005. He continued research work at VCU and will complete his Master of Science degree in August 2006, after which he will matriculate as a medical student in the class of 2010 at VCU School of Medicine. He was recently accepted by the Phi Kappa Phi Honor Society.